Drosophila ovarian germline stem cell cytocensor projections dynamically receive and attenuate BMP signalling

Scott G. Wilcockson[1] and Hilary L. Ashe[1]*

Affiliations: [1]Faculty of Biology, Medicine and Health, University of Manchester, Manchester, M13 9PT, UK.

*Correspondence: hilary.ashe@manchester.ac.uk

KEYWORDs

BMP signalling, Drosophila, germline stem cell, cytoskeleton, niche, Dpp, Tkv, signalling filopodia

SUMMARY

In the *Drosophila* ovarian germline, BMP signals released by niche cells promote germline stem cell (GSC) maintenance. Although BMP signalling is known to repress expression of a key differentiation factor, it remains unclear whether BMP-responsive transcription also contributes positively to GSC identity. Here, we identify the GSC transcriptome using RNA-seq, including the BMP-induced transcriptional network. Based on these data, we provide evidence that GSCs form two types of cellular projections. Genetic manipulation and live *ex vivo* imaging reveal that both classes of projection allow GSCs to access a reservoir of Dpp held away from the GSC-niche interface. Moreover, the microtubule-rich projections, termed 'cytocensors', formed downstream of BMP have additional functionality, which is to attenuate BMP signalling, allowing dynamic modulation of signal transduction to facilitate differentiation following GSC division. We propose that cytocensors will be synthesised by other types of cells in diverse contexts to calibrate signalling responses.

INTRODUCTION

The stem cell niche is a tissue microenvironment, specialised in structure and function, that ensures the self-renewal and survival of cells needed to maintain tissue homeostasis throughout an organism's life (Hsu and Fuchs, 2012). The first niche was characterised in the *Drosophila* ovarian germline (Cox et al., 1998; King and Lin, 1999) where the Bone Morphogenetic Protein (BMP) family member, Decapentaplegic (Dpp), was found to be necessary for maintenance of germline stem cells (GSCs) (Xie and Spradling, 2000, 1998). Since this discovery, there has been an explosion in the identification and characterisation of stem cell niches in most tissues and model organisms. As well as providing a home for stem cells in which they can sustain their multipotency and self-renewal capabilities, the niche also provides an important conduit through which stem cells can respond to both local and systemic signalling (Ables and Drummond-Barbosa, 2017; Peck et al., 2017). Dysregulation of niche signalling and stem cell maintenance is associated with a plethora of human diseases (Hoggatt et al., 2016; Li and Jasper, 2016; Mashinchian et al., 2018).

Within the *Drosophila* ovary, GSCs are maintained at the anterior tip in discrete structures referred to as germaria (Fig. 1A; Lin and Spradling, 1993). A small population of somatic cells, the Cap cells (CpCs), contact the GSCs through E-cadherin-based adherens junctions (Song et al., 2002) and promote stem cell identity through the secretion of Dpp homodimers or Dpp-Glassbottom boat (Gbb) heterodimers (Song et al., 2004). Dpp signals at exquisitely short-range to maintain only 2-3 GSCs per niche (Wilcockson et al., 2017). Upon cell division, one daughter cell exits the niche, allowing it to move out of the range of the Dpp signal and differentiate. Multiple mechanisms have been described for restricting Dpp range, including stabilisation or concentration of Dpp within the niche by the heparan sulphate proteoglycan Divisions abnormally delayed (Dally), sequestration by a collagen IV matrix in between the GSCs and niche cells, and escort cell expression of the Dpp receptor, Thickveins (Tkv), which acts as a 'decoy' to soak up any BMP ligand that escapes the niche (Wilcockson et al., 2017).

Within GSCs, the BMP signal is transduced through the canonical pathway resulting in the phosphorylation and activation of the Smad1/5 ortholog, Mothers against Dpp (Mad). Mad oligomerises with the Smad4 ortholog Medea leading to their nuclear accumulation (Hamaratoglu et al., 2014). A key Dpp target gene in GSCs is *bag of marbles* (*bam*), encoding an essential differentiation factor, which is repressed by Dpp signalling (Chen and McKearin, 2003; Song et al., 2004). Upon cell division, the daughter cell that exits the niche derepresses *bam,* which initiates the differentiation programme. However, other than *bam*, only a handful of Dpp target genes in GSCs have been identified (Casanueva and Ferguson, 2004; Xia et al., 2012) and there is little understanding of how the BMP self-renewal signal may positively act on GSC identity. Therefore, we used RNA-seq to identify the GSC transcriptional network, including genes that are regulated by the Dpp signal. These data reveal that the GSC synthesises different types of cellular projections that function to receive the niche BMP signal, including one class that also plays an active role in BMP signal attenuation, which we thus refer to as 'cytocensors'. This ability to fine-tune signalling identifies a new property for dynamic signalling projections, which have previously only been implicated in sending and receiving signals.

RESULTS

RNA-seq of GSC-like cells and CBs reveal putative GSC self-renewal and maintenance factors

To identify novel regulators of GSC self-renewal and differentiation, we purified GSCs and CBs and compared their transcriptomes. In the absence of a GSC-specific marker, we genetically expanded the population by expressing constitutively active Tkv (*UASp-tkv^{QD}*) using a maternal germline *Gal4* driver (*nos-Gal4::VP16*) (Fig. 1B). This results in the formation of tumours of pMad^{+} GSC-like cells. FACS enabled isolation of germ cells from the surrounding soma. CBs were isolated as single cells expressing a *bam.GFP* reporter (Fig. 1C, Chen & Mckearin, 2003) and GSC-like cells based on their expression of the germ cell marker *vasa^{GFP}* (Fig. 1D, Sano, Nakamura, & Kobayashi, 2002). Differential expression analysis revealed 2,249 differentially expressed genes with just under one third up-regulated in *tkv^{QD}* (GSCs) and around two thirds up-regulated in *bam.GFP* expressing cells (CBs) (Fig. 1E), including *Dad* and *bam*, respectively (Supplementary Figure 1). GO term analysis of GSC-enriched transcripts reveals biological processes associated with gonad development, chromatin organisation and transcription, whereas those identified for CB-enriched transcripts indicate a change in cellular metabolism and up-regulation of genes associated with growth and protein production (Fig. 1F). We also find GSC enrichment of transcripts associated with nervous system development and cell migration. These include adhesion proteins (*Nrg, Liprin-α, Ten-m,* and *ckn*), axon guidance molecules (*PlexB*, *Sema-2a*, *robo*, and *sli*), ciliogenesis factors (*Rfx*, *nuf*, *Oseg2*, and *Cc2d2a*), and structural/cytoskeletal proteins (*hts*, *β-spec*, *Dlic*, *stai*, *patronin*, and *futsch*).

To identify the genes specifically regulated by Dpp signalling, we used germline-specific RNAi knockdown of *bam* expression (*UASp-bam^{shRNA}*), which blocks differentiation. Stem cells continue to divide resulting in the formation of a tumour of pMad-negative GSC-like cells that can again be isolated through *vasa^{GFP}* expression (Fig. 1G). Differential expression analysis of *tkv^{QD}* and *bam^{shRNA}* expressing

GSC-like cells reveals around 300 genes differentially regulated by Dpp signalling, with just under half the genes up-regulated in response to Dpp (Fig. 1H). GO term analysis suggests that Dpp signalling promotes expression of genes associated with transcription, differentiation and growth, while down-regulating genes associated with metabolic processes and protein production (Fig. 1I). Again, we find a set of genes up-regulated by Dpp signalling involved in nervous system development and synapse organisation, including the genes that encode the master ciliogenesis transcription factor *Rfx* and the MAP1B homolog *Futsch*.

These data reveal the changing landscape of the germline transcriptome, from self-renewing GSCs to differentiating daughter CBs. Within this transcriptome we have identified the Dpp-responsive network, which includes the *Rfx* and *Futsch* genes that are both known to regulate the formation of microtubule (MT)-based structures.

Germline stem cells extend MT- and actin-rich projections into the niche

To investigate a potential cytoskeletal response to Dpp signalling in GSCs, we first defined the stem cell MT network using immunofluorescence staining of tyrosinated α-tubulin (a marker of new, dynamic MTs), acetylated α-tubulin (a marker of stable MTs), and the germ cell marker, Vasa. GSCs are enriched for tyrosinated α-tubulin compared to the post-mitotic CpCs (Fig. S1a, CpCs marked by asterisks). This difference enables the visualisation of stem-derived MT-rich projections that a subset of GSCs can be seen extending into the niche. The cytoplasmic protein, Vasa, also localises within these projections, further confirming that these structures are GSC-derived. To further characterise these MT-rich projections, we specifically visualised the stem cell MT network through the germline expression of *UASp-eGFP.αTubulin84B* (*GFP.αTub*). Immunofluorescence staining of the adherens junction protein, E-cadherin, delineates the contact points between individual cap cells and the GSC-niche interface. Indeed, a subset of GSCs generate single, short MT-based projections that appear to extend around or between the CpCs (Fig. 1J and S1D).

Our RNA-seq data identified a number of stem cell enriched genes associated with ciliogenesis. We therefore addressed whether these MT-rich projections were ciliary in nature. GFP.αTub^{+} projections are composed of acetylated microtubules, a classic ciliary marker (Fig. S1B and Bi). However, they show a non-uniform pattern of acetylation unlike stable ciliary MTs. In addition, no association of these GSC projections with the centrosome based on γ-tubulin staining is observed (Fig. S1C). Based on these observations we propose that these GSC MT-rich projections are not ciliary in nature and here on refer to them as ‘cytocensors’ based on their signal suppression property, ie acting as a censor (see later). They do appear similar to recently described MT-based nanotubes generated by the GSCs of the *Drosophila* testis whose formation is regulated by ciliary proteins (Inaba et al., 2015). However, our data highlight numerous differences between cytocensors and MT-nanotubes, indicating that these are distinct structures (see Discussion).

Immunofluorescence imaging of the MT associated protein Futsch, which is up-regulated in response to Dpp signalling, reveals strong GSC enrichment compared with CpCs (Fig. 1K). Futsch function is best characterised in the nervous system where it promotes MT stability (Halpain and

Dehmelt, 2006). Futsch co-localises extensively with the stem cell MT network, including the cytocensor MTs, suggesting that Futsch may play a role in stem cell projection stability (see later). We next addressed whether these projections contain or require the actin cytoskeleton for their formation by expressing both *GFP.αTub* and *UASp-Actin5C.mRFP* specifically in the germline. Immunofluorescence staining reveals that GSCs also generate multiple actin-based projections (APs). In Figure 1L, a single stem cell can be seen to form two distinct projections; one short actin-based filopodium (magenta arrowhead) and a longer projection containing both MTs and actin (green arrowhead). This shows that GSC cytocensors are both MT- and actin-rich projections while GSCs also generate additional APs.

To investigate the regulatory relationship between actin and MTs in the formation of GSC projections, we performed *ex vivo* treatment of *Drosophila* ovaries with cytochalasin D and nocodazole, inhibitors of actin and MT polymerisation, respectively. A short 30 min incubation with 2µM cytochalasin D was sufficient to reduce F-actin levels and results in the accumulation of globular actin puncta in the cytoplasm (Figure S1E). Similarly, a 30 min incubation with 10µM nocodozole reduced tubulin levels. Treatment of ovaries expressing germline *UASp-Act42D.GFP* with cytochalasin D significantly reduces the number of niche-directed APs while treatment with nocodazole had no effect (Fig. 1M). Conversely, treatment of *GFP.αTub* expressing ovaries with both drugs resulted in a significant reduction in the ability of GSCs to generate cytocensors, in comparison with DMSO-treated ovaries. This suggests that APs form independently of the MT network, however, the formation of cytocensors is dependent on actin. In addition, APs are much more abundant than cytocensors (Fig. 1M, compare DMSO controls). These data therefore suggest that APs may represent the primary structure from which cytocensors ultimately emanate.

Projections dynamically probe the niche microenvironment

The enrichment of tyrosinated MTs and the non-uniformity of α-tubulin acetylation suggests that the cytocensors may be dynamic in nature. To determine if this is the case, we used live imaging to monitor MT dynamics in *GFP.αTub* expressing GSCs *ex vivo*. This allows the imaging of GSCs that can be seen to extend cytocensors that dynamically probe the niche microenvironment over the course of 1-2 hours (Movie S1). Figure 2A shows frames from Movie S1 that focuses on a single motile cytocensor extended into the niche that collapses and reforms multiple times over the course of imaging. This shows that cytocensors are relatively dynamic in nature. We similarly visualised F-actin by driving germline expression of *UASp-LifeAct.eGFP* (Movie S2). Strong labelling of cortical F-actin is seen at the GSC-niche interface from which the APs emerge (Fig. 2B). The GSCs generate short filopodia-like projections that extend into the niche and although they appear dynamic, they do exhibit a long lifetime (compare Fig. 2Bi and ii). In addition, some GSCs extend broad lamellipodia-like projections that extend over or in between multiple niche cells (Fig. 3Ci and Movie S3), and individual finger-like filopodia can be seen to extend from the ends of these structures (Fig. S3 and Movie S4). We also found additional transient lateral GSC projections (Movie S3) while all early differentiating germ cells (CBs, 2-cell cysts, and 4-cell cysts) generate long, transient APs (Fig. 2Cii).

To compare the nature of these projections, we grouped those that extend into the niche ($GSC^{<45°}$; point of nucleation occurs at <45° relative to the centre of the niche (0°)) and lateral projections ($GSC^{>45°}$; point of nucleation occurs at >45° is defined as a lateral projection) together and compared these to the projections generated by the differentiating cells (Fig. 2D). GSC projection formation appears polarised as most APs are nucleated in the direction of the niche, or below 90°, while CBs tend to generate projections at any angle >45°. This may simply be due to structural hinderance, with the presence of neighbouring GSCs precluding the formation of niche-directed CB projections.

Comparing the length, lifetime, and speed of filopodia extension and retraction reveals that $GSC^{<45°}$ projections are significantly shorter, slower and more stable than $GSC^{>45°}$ projections (Fig. 2F-I). These lateral projections are more similar to those formed by the CBs and 2-cell cysts which are generally longer, the extent of which increases as differentiation progresses (Fig. 2F), are significantly more transient/unstable, indicated by their short lifetime (Fig. 2G) and their speed of growth and collapse (Fig. 2H and I). Together these data show that GSC projections are dynamic and probe the niche microenvironment. In addition, the formation of unstable APs is a common trait of early germ cells, while GSCs also extend more stable, short APs into the niche.

Cytocensors form in response to Dpp signalling

Our RNA-seq data suggest that Dpp signalling regulates the expression of *Futsch* and *Rfx*, while GSCs also showed general enrichment of other cytoskeletal- and ciliogenesis-associated factors. Therefore, germline-specific RNAi was used to test the role of a subset of these genes in cytocensor formation. We firstly focused on the MT-stabiliser Futsch and the tubulin-binding protein Stathmin (Stai). $futsch^{shRNA}$ expression (Fig. 3Ai) significantly reduces the frequency of cytocensors formed, while those that are formed are much shorter compared to wildtype projections. Conversely, $stai^{shRNA}$ expression leads to significantly longer and thicker projections. We also knocked down expression of Klp10A, a MT-depolymerising kinesin shown to regulate MT-nanotube formation and centrosome size in male GSCs (Chen, Inaba, Venkei, & Yamashita, 2016; Inaba et al., 2015) (Fig. 3Aiii). This also leads to significantly longer and slightly thicker projections than wildtype projections. Klp10A does not however appear to regulate female GSC centrosome size (Figure S3A and Ai).

We next addressed the roles of four genes associated with ciliogenesis including *Rfx* and *nuclear fallout* (*nuf*). Rfx^{shRNA} expression leads to a significant decrease in the frequency of cytocensor formation (Fig. 3D), while those that are formed appear normal. nuf^{shRNA} expression had no effect on the length, thickness or frequency of projection formation. Two intraflagellar transport proteins were also included in our analysis, Oseg6 and IFT52. Although they do not show enrichment they are expressed in GSCs and CBs and function downstream of Rfx (Laurençon et al., 2007). $Oseg6^{shRNA}$ expression results in longer cytocensors that can often be found to contain a globular accumulation of tubulin at the tip (Fig. 3Aiv), while $IFT52^{shRNA}$ expression resulted in a small increase in the frequency of cytocensors formation. Together, these data reveal a set of factors, two of which are up-regulated by Dpp signalling (Futsch and Rfx), that regulate cytocensor formation.

Given the necessity of actin for the formation of cytocensors, we examined three actin cytoskeletal components and known regulators of filopodia and cytoneme formation; the formin diaphanous (dia), SCAR, and filamin *(*cheerio*,* cher) (González-Méndez et al., 2017; Roy et al., 2014). *dia*^{shRNA} expression results in complete loss of the germline, therefore the effect on cytocensor formation could not be determined. However, knockdown of either *SCAR* or *cher* expression resulted in the formation of abnormally long and thick projections (Fig. 3Av-C). These results further highlight the role of actin in the formation of cytocensors.

GSCs are extremely sensitive to Dpp signalling levels, making it difficult to specifically manipulate signalling pathway proteins without triggering differentiation. Therefore, to confirm that cytocensors form in response to Dpp signalling we examined heterozygous mutants for either the ligand *(dpp*$^{hr92/+}$), receptor (*tkv*$^{7/+}$), or R-Smads (*mad*$^{1-2/+}$ and *med*$^{13/+}$), representing sensitized backgrounds where stem cells experience lower Dpp signalling. All heterozygous mutants show a significantly reduced ability to form projections with *mad*$^{1-2/+}$ causing the greatest loss (Fig. 3E and F). In addition, the cytocensors that are formed are frequently abnormal, particularly longer and thicker than controls (Fig. 3G and H). These results show that the frequency of cytocensor formation correlates with the ability of GSCs to receive and transduce Dpp signalling. We addressed whether ectopic Dpp could induce cytosensor formation. Cells that exit the niche do not typically generate cytosensors (Fig. S3B). Prevention of ColIV deposition in the niche by larval haemocytes (*HmlΔ-Gal4 > vkg*^{shRNA}) extends Dpp signalling range, resulting in the accumulation of ectopic GSC-like cells (Fig. S3C; Van De Bor et al., 2015). These cells extend cytocensors, suggesting that Dpp signalling is both necessary and sufficient to induce cytocensor formation.

CpC-presentation of Dally generates a reservoir of Dpp

GSCs may extend cellular projections into the niche to increase the GSC surface area in contact with the niche to augment Dpp signal reception. We therefore examined the localisation of Dpp around the niche using endogenous Dpp tagged with mCherry (Dpp^{mCh}), in the same position as the previously described Dpp^{GFP} (Teleman and Cohen, 2000). Using immunofluorescence to label only extracellular Dpp^{mCh} and E-cadherin, which outlines CpCs, we detect Dpp^{mCh} concentrated in puncta to the anterior of the niche creating an anterior to interface high gradient (Fig. 4A and Ai). This same localisation pattern is also observed using two previously described Dpp transgenic lines tagged with either HA (Fig. S4A, Shimmi, Umulis, Othmer, & O'Connor, 2005) or GFP (Fig. S4B, Teleman & Cohen, 2000).

We also visualised the localisation of endogenous Dally, tagged with mCherry (Dally^{mCh}), which is expressed by CpCs. Similar to Dpp, we find an anterior to interface high gradient of punctate extracellular Dally^{mCh} (Fig. 4B and Bi). To address whether Dally regulates Dpp distribution, the Gal80^{ts} system was used to temporally induce the knockdown or overexpression of Dally in niche cells. In adult flies raised at 18°C, Gal80^{ts} represses Gal4 activity and therefore expression of the associated transgene. In adult flies raised at 29°C, Gal80^{ts} is repressed enabling transgene expression. When *Dally*^{shRNA} or *Dally*^{OE} flies are raised at 18°C for 3 days, Dpp^{mCh} shows an anterior to interface high gradient (Fig. S4B and C). In contrast, *Dally*^{shRNA} flies raised at 29°C for 3 days (inducing knockdown)

have equivalent levels of Dpp^{mCh} on both sides of the niche and an average anterior to interface ratio of one (Fig. 4C) indicating a loss of the Dpp gradient. When Dally overexpression flies are raised at 29°C for 3 days, the opposite effect is observed as Dpp^{mCh} further accumulates in the anterior region resulting in a steeper gradient with a higher average anterior to interface ratio (Fig. 4C). Together these data show that niche expressed Dally binds and sequesters secreted Dpp away from the GSC-niche interface. This leads to the formation of a reservoir of Dally-bound Dpp and an anterior high gradient of extracellular Dpp.

GSC projections access Dally-Dpp and form platforms for Dpp signal transduction

As Dpp is concentrated away from GSCs, we addressed where Tkv activation occurs using a fluorescent reporter of ligand-receptor interaction, TIPF (Michel et al., 2011). Using the endogenous fluorescence of germline expressed TIPF (*Bam27::TIPF*), we found the majority of active Tkv co-occurs with Dally^{mCh} (Fig. 4D and Di). This suggests that Dally-bound Dpp is the key source of ligand for GSCs and that signalling likely occurs on GSC projections that are extended into the niche. To test the role of Dally in promoting Dpp-Tkv interaction, we counted the number of TIPF puncta per niche following manipulation of Dally in niche cells, as described previously. Transient induction of *Dally^{shRNA}* expression for 3 days resulted in a decrease in the number of TIPF puncta compared to controls (18°C; Fig. 4E and F). Conversely, inducing *Dally* overexpression for 3 days results in an increase in niche TIPF puncta, compared to flies raised at 18°C. These results are consistent with Dally-bound Dpp being the major source of this self-renewal signal for GSCs and the extension of projections enables access to Dpp (Fig. 4G).

To determine if the signalling machinery could be visualised on GSC projections, the localisation of endogenous Tkv tagged with mCherry (Tkv^{mCh}) was monitored on APs using germline expression of *LifeAct.GFP* (Fig. 5A). Tkv^{mCh} can be detected at the GSC-niche interface and at the base of short APs. Upon extension into the niche, Tkv^{mCh} localises along the projection (magenta arrowhead), suggesting that APs could function as signalling platforms for Dpp signalling. In addition, Tkv^{mCh} is also found decorating lateral GSC projections (Fig. S5). In the same way Tkv^{mCh} localisation was monitored in *GFP.αTub* expressing germline stem cells (Fig. 5B). Here large puncta of Tkv^{mCh} were detected trafficking onto cytocensors and accumulating at the tip. To determine whether these projections contact the Dpp reservoir, Dpp^{mCh} was visualised with *GFP.αTub* (Fig. 5C). Cytocensors can be seen to form stable contacts with Dpp^{mCh} puncta. Finally, in order to determine whether the Tkv localising to GSC projections is active, we used germline expression of *UASp-FTractin.dTomato* to visualise actin filopodia alongside TIPF. In Figure 5D a single TIPF puncta is shown localised to the base of a pre-existing filopodium. The projection collapses and at 1:12 min has reformed. At this point a TIPF puncta appears at the tip of the AP and gradually moves toward the base. These data show that APs are sites of active Dpp signalling as Tkv activation can be seen to occur at the tip of projections.

Dia-regulates actin projection formation and Dpp signal reception

To determine the requirement for projections in GSC Dpp signalling, we firstly returned to the actin polymerising factor Dia which we previously found to be necessary for GSC maintenance (Fig. 2). By

raising *dia*^{shRNA} flies at 18°C shRNA expression is repressed during larval development (Fig. 6A and B). Adults maintained at 18°C for 3 days do exhibit some GSC loss, suggesting there is some leaky shRNA expression and highlighting the sensitivity of GSCs to slight changes in *dia* levels. When flies are shifted to 25°C for 3 days, rapid GSC loss is observed in line with our previous results (Fig. 6A and B). To determine if stem cell loss is due to perturbed Dpp signalling, immunostaining for pMad was used as a readout of the Dpp signalling response. When *dia*^{shRNA} expression is induced by shifting adult flies to 25°C for 3 days, GSCs begin exhibiting greater variability in pMad levels. Typically, one GSC per niche experiences slightly higher levels of pMad than its neighbour (Fig. 6C and D). *dia*^{shRNA} expression results in a significant increase in the variability of pMad levels between neighbouring stem cells. Previous studies have shown that Dpp signalling mutant clones are outcompeted by neighbouring wildtype GSCs, lost from the niche and replaced by symmetric cell division (Song et al., 2004; Xie and Spradling, 1998). The disparity in Dpp signalling response seen with *dia*^{shRNA} expression could similarly be expected to promote such competition. However, what we observe is an increase in GSC loss and an increased proportion of niches occupied by single stem cells (Fig. 6A and B). *dia*^{shRNA} expression also blocks cytokinesis resulting in single large polyploid GSCs (Fig. 6F) suggesting that lowering *dia* expression induces GSC competition, however, the 'winner' cells cannot replenish the niche through symmetric cell division and so take over the niche.

We next determined whether Dia regulates actin-projection formation using *LifeAct.GFP* expression to label F-actin. *dia*^{shRNA} expression resulted in an overall decrease in the number of GSCs extending projections into the niche (Fig. 6E), whereas the projections that remain are abnormal. While wildtype projections are thin, finger-like filopodia (Fig. 6Hi), or broader lamellipodia (Fig. 2C), *dia*^{shRNA} GSCs extend branched, thick projections (Fig. 6Ii). Furthermore, their formation appears disorganised with the extension of supernumerary lateral projections (compare Fig. 6Hii and Iii). These data suggest that Dia regulates AP formation in GSCs. Uneven knockdown of *dia* expression generates 'winner' cells that exhibit disorganised and branched APs that potentially increase Dpp uptake, increasing pMad levels and leading these cells to outcompete their neighbours for niche occupancy.

Cytoskeletal projections are necessary for Dpp signal activation and attenuation

These results show that increased AP formation is associated with increased receptivity to niche signalling. If cytoskeletal projections are necessary for GSCs to access the Dpp reservoir, as our data suggests, we would predict that inhibiting projection formation would compromise signal reception. To test this, germaria were again treated with cytochalasin D or nocodozole *ex vivo* to inhibit projection formation and the number of TIPF puncta in and around the niche was used as a readout of Dpp signal reception. Germaria treated with DMSO maintained similar levels of signal activation after 30 and 90 mins of treatment (Fig. 7A). Treatment with cytochalasin D, however, results in a significant reduction in TIPF puncta even after 30 mins (Fig. 7A and Ai providing further evidence that the APs are necessary for Dpp signal reception in GSCs. Treatment with nocodozole for 30 mins had no effect on the average number of TIPF puncta, suggesting that in the absence of cytocensors GSCs are still able to access and receive Dpp through APs. However, there is a significant increase in the number of TIPF puncta following a longer nocodazole treatment (Fig. 7A), consistent with the absence of cytocensors leading

to overactive signalling. This suggests that cytocensors are necessary for attenuating Dpp signal transduction.

To investigate this further, we returned to some of the earlier described regulators of cytocensor formation. To examine their function in Dpp signal transduction, pMad staining was again used as a readout of Dpp signal transduction. We also assayed for an effect on GSC maintenance/differentiation by counting the number of early germ cells. RNAi-knockdown of *IFT52* or *klp10A,* which increases the frequency of projection formation or enhances the growth of cytocensors, respectively, leads to an increased rate of GSC loss (Fig. 7B and C) associated with a decrease in pMad levels (Fig. 7D). This suggests that enhancing cytocensor formation or length is detrimental to the maintenance of pMad activation, such as through mis-trafficking of Tkv on long projections. Although *nuf*^{shRNA} had no effect on cytocensor formation, it does lead to an increase in the number of early germ cells and is associated with increased pMad levels. Expression of *Oseg6*^{shRNA}, however, had no effect on early germ cell number or pMad levels. RNAi knockdown of *futsch* or *Rfx*, which in both cases disrupts cytocensor formation, results in ectopic early germ cells (Fig. 7B and C). This phenotype is typically associated with a delay in the rate of differentiation. Consistent with this, in both cases we also detect a significant increase in GSC pMad levels (Fig. 7D). These data suggest that cytocensors play an additional critical role in the attenuation of stem cell Dpp signalling, which allows GSCs to establish a pMad level that facilitates differentiation following niche exit.

DISCUSSION

Here we present data describing the changing transcriptome of GSCs as they transition from self-renewal to differentiation. Genes up-regulated in GSCs are associated with gonad development, chromatin organisation and transcriptional regulation. This is consistent with germline differentiation being accompanied by a reduction in transcriptional activity (Flora et al., 2018; Zhang et al., 2014) and altered chromatin organisation (Flora et al., 2017). Genes upregulated in CBs include those encoding factors involved in cellular metabolism, growth and protein production. This can be rationalised with CB biology as, upon exiting the stem cell niche, CBs quickly undergo 4-rounds of mitosis to generate a 16-cell cyst and this transition is associated with an increase in general and mitochondrial protein synthesis (Sanchez et al., 2016; Teixeira et al., 2015). We also identified new Dpp target genes in GSCs and have elucidated the function of two positive Dpp targets, *Rfx* and *futsch*, which promote synthesis of cytocensors along with other MT-associated genes in the GSC transcriptome.

Based on our data, we propose a model whereby the GSC synthesises APs which access the Dally-bound reservoir of Dpp to receive the signal (Fig. 7E). In support of this, short-term inhibition of AP formation significantly reduces active Tkv levels, whereas increasing AP branching and disorganisation (*dia*^{shRNA}) is associated with increased pMad levels and competitiveness in some GSCs. Presumptive ‘loser’ stem cells, with lower pMad levels and/or loss of niche-directed projections, are subsequently outcompeted for niche occupancy. We propose that, following activation of Dpp target

genes, such as *Rfx* and *futsch*, these APs develop into cytocensors (Fig. 7E). We provide evidence that, like the APs, these cytocensors access Dally-bound Dpp localised away from the GSCs.

These GSC projections are acting at much shorter range than that typically described for signalling filopodia, which have been identified in many contexts associated with the regulation of long-range signal transduction (Wilcockson et al., 2017). For example, cytonemes in the larval wing disc and dorsal air sac primordium drive long-range Dpp signalling (Huang and Kornberg, 2016; Roy et al., 2014). We suggest that the advantage of the unusual GSC-niche architecture, whereby GSC projections collect signal from a pool that accumulates on the opposite side of adjacent CpCs, may be two-fold. Firstly, it concentrates the potent Dpp self-renewal signal further away from the GSCs, guarding against ectopic Dpp diffusion that would disrupt GSC differentiation. Secondly, and we suggest more importantly, our data provide evidence that the cytocensors allow GSCs to actively regulate their Dpp signalling levels by both collecting the Dpp signal and attenuating its transduction (Fig. 7E). Perturbation of cytocensors, through genetic manipulation or drug treatment, leads to increased pMad levels and active Tkv, respectively (Fig. 7E). Although extending the length or frequency of cytocensors leads to lower pMad levels and GSC loss, we propose that this is due to a failure to traffic active Tkv back to the GSC body Therefore, we propose that these cytocensors promote feedback inhibition that maintains signal transduction at a threshold that facilitates differentiation following GSC division (Fig. 7E). Mathematical modelling has previously shown that the pMad concentration prior to division is important, so that pMad falls below a critical level in the GSC daughter that exits the niche, allowing *bam* derepression and differentiation (Harris et al., 2011).

How might cytocensors facilitate Dpp signal termination? In the primary cilium, TGFβRI and II are localised within the cilium where, upon ligand binding, they move to the ciliary base and activate receptor-Smads (Clement et al., 2013; Pedersen et al., 2016). The inhibitory Smad, Smad7, which targets TGFβR for degradation, also concentrates at the base the cilium where it inhibits TGFβR-Smad interaction to modulate signalling levels. The ubiquitin ligase Smurf, which recruited by Smad7, is also known to localise to the cilium. We speculate that cytocensors will act as a hub where GSCs can concentrate negative regulators, such as Dad and Smurf, to efficiently modulate pMad levels. pMad levels increase when cytocensors are disrupted, yet under such conditions the APs remain, suggesting that the cell can receive but not regulate Dpp signal transduction via APs. If, as proposed, the cytocensor acts as a hub for the negative regulation of signalling, failure of the APs to terminate signalling may reflect the absence of regulatory factors at these projections.

This signal attenuating activity of female cytocensors is in stark contrast to the role of male MT-nanotubes, which function to increase the stem cell-niche interface area to specifically increase Dpp signal transduction. Perturbing nanotube formation decreases pMad levels, increasing the rate of competition-induced loss. Furthermore, male and female projections exhibit several structural differences. Male projections are MT-based static structures lacking actin, and most GSCs (~80%) extend one or more of these projections into the body of neighbouring niche cells (Inaba et al., 2015). Female cytocensors, on the hand, are rich in both MTs and actin, are relatively dynamic, probing around and in between niche cells, and much less frequently found (~40% of GSCs generate a single

projection). The distinct nature of male and female projections may reflect differing requirements for Dpp signalling in stem cell maintenance or more limiting Dpp levels and the competition between GSCs and somatic cyst stem cells for niche occupancy in the testis (Greenspan et al., 2015).

Given our evidence for signal transduction through GSC projections, this raises the question as to whether GSCs can receive Dpp in their absence. Monitoring Dpp-Tkv interaction following cytochalasin D treatment shows that TIPF puncta are still present up to 90 min after treatment. This may suggest that Dpp that escapes the reservoir can drive low-level signal transduction. Alternatively, the maintenance of a few puncta could be due to perdurance of the TIPF reporter or disrupted trafficking/endocytosis of Tkv that was active prior to treatment (Lamaze et al., 1997). The identification of additional actin regulators involved in this process will be necessary to determine the absolute requirement for APs in GSC Dpp signalling. One putative factor is the small GTPase Rac1, a key regulator of the formation and identity of APs, which concentrates at the GSC-niche interface (Lu et al., 2012). Rac1 is necessary for long-term GSC maintenance and was suggested to promote BMP signal transduction.

In addition, we also find lateral GSC and CB projections decorated with Tkv^{mCh}. It has been shown that differentiating germ cells remain highly sensitive to 'leaky' Dpp, while ectopic Dpp can induce germ cell dedifferentiation (Xie and Spradling, 1998). The formation of these projections may therefore promote the sensitisation of germ cells to Dpp signalling, enabling their dedifferentiation to replace GSCs lost during aging or stress (Cheng et al., 2008; Kai and Spradling, 2004).

Dynamic signalling projections play important roles in enabling the receipt or delivery of signalling molecules over large distances or between cells of different tissues. Our data describe a new role for such projections in the modulation of signal transduction that may be of particular importance to adult stem cells. These are cells that need to be sensitive to local and systemic signalling while still maintaining their own plasticity. Therefore, the ability to precisely control signalling levels through similar cellular projections would allow for precision in stem cell self-renewal and differentiation. While signalling projections are common during development, it remains to be determined whether they are also commonly found in adult stem cells. However, in the murine gut, intestinal stem cells have previously been shown to extend apical processes that reach in between neighbouring Paneth cells that constitute a key part of the intestinal stem cell niche (Barker et al., 2007). Also, the intestinal stem cell markers and GPCRs, Lgr4/5, have been shown *in vitro* to drive formation of cytoneme-like projections (Snyder et al., 2015). It will be interesting to determine the role of these projections in stem cell signalling and whether cytocensors are found in other stem cell systems.

ACKNOWLEDGEMENTS

We thank Ryo Hatori and Thomas Kornberg for Dpp.mCh and Tkv.mCh flies, and Georgios Pyrowolakis, the Bloomington Drosophila Stock Center and the Developmental Studies Hybridoma Bank for flies and/or antibodies. We thank Jens Januschke for advice on live imaging. We also thank Catherine Sutcliffe and Rosalind Wilkes for technical assistance, University of Manchester Genomic

Technologies Facility and Ping Wang for analysis of RNA-seq data. This work was supported by a BBSRC PhD Studentship.

AUTHOR CONTRIBUTIONS

Conceptualisation, S.G.W, H.L.A; Methodology, S.G.W, H.L.A; Investigation, S.G.W; Formal Analysis, S.G.W; Writing, S.G.W, H.L.A; Supervision, H.L.A; Funding Acquisition, H.L.A.

DECLARATION OF INTERESTS

The authors declare no competing interests.

REFERENCES

Ables, E.T., and Drummond-Barbosa, D. (2017). Steroid Hormones and the Physiological Regulation of Tissue-Resident Stem Cells: Lessons from the Drosophila Ovary. Curr. Stem Cell Reports *3*, 9–18.

Barker, N., van Es, J.H., Kuipers, J., Kujala, P., van den Born, M., Cozijnsen, M., Haegebarth, A., Korving, J., Begthel, H., Peters, P.J., et al. (2007). Identification of stem cells in small intestine and colon by marker gene Lgr5. Nature *449*, 1003–1007.

Casanueva, M.O., and Ferguson, E.L. (2004). Germline stem cell number in the Drosophila ovary is regulated by redundant mechanisms that control Dpp signaling. Development *131*, 1881–1890.

Chen, D., and McKearin, D. (2003). Dpp Signaling Silences bam Transcription Directly to Establish Asymmetric Divisions of Germline Stem Cells. Curr. Biol. *13*, 1786–1791.

Chen, C., Inaba, M., Venkei, Z.G., and Yamashita, Y.M. (2016). Klp10A, a stem cell centrosome-enriched kinesin, balances asymmetries in Drosophila male germline stem cell division. Elife *5*, 1–14.

Cheng, J., Türkel, N., Hemati, N., Fuller, M.T., Hunt, A.J., and Yamashita, Y.M. (2008). Centrosome misorientation reduces stem cell division during ageing. Nature *456*, 599–604.

Clement, C.A., Ajbro, K.D., Koefoed, K., Vestergaard, M.L., Veland, I.R., HenriquesdeJesus, M.P.R., Pedersen, L.B., Benmerah, A., Andersen, C.Y., Larsen, L.A., et al. (2013). TGF-β Signaling Is Associated with Endocytosis at the Pocket Region of the Primary Cilium. Cell Rep. *3*, 1806–1814.

Cox, D.N., Chao, A., Baker, J., Chang, L., Qiao, D., and Lin, H. (1998). A novel class of evolutionarily conserved genes defined by *piwi* are essential for stem cell self-renewal. Genes Dev. *12*, 3715–3727.

Flora, P., McCarthy, A., Upadhyay, M., and Rangan, P. (2017). Role of Chromatin Modifications in Drosophila Germline Stem Cell Differentiation. In Signaling-Mediated Control of Cell Division : From Oogenesis to Oocyte-to-Embryo Development, S. Arur, ed. (Cham: Springer International Publishing),

pp. 1–30.

Flora, P., Schowalter, S., Wong-Deyrup, S.W., DeGennaro, M., Nasrallah, M.A., and Rangan, P. (2018). Transient transcriptional silencing alters the cell cycle to promote germline stem cell differentiation in Drosophila. Dev. Biol. *434*, 84–95.

González-Méndez, L., Seijo-Barandiarán, I., and Guerrero, I. (2017). Cytoneme-mediated cell-cell contacts for Hedgehog reception. Elife *6*.

Greenspan, L.J., de Cuevas, M., and Matunis, E. (2015). Genetics of Gonadal Stem Cell Renewal. Annu. Rev. Cell Dev. Biol. *31*, 291–315.

Halpain, S., and Dehmelt, L. (2006). The MAP1 family of microtubule-associated proteins. Genome Biol. *7*, 1–7.

Hamaratoglu, F., Affolter, M., and Pyrowolakis, G. (2014). Dpp/BMP signaling in flies: From molecules to biology. Semin. Cell Dev. Biol. *32*, 128–136.

Harris, R.E., Pargett, M., Sutcliffe, C., Umulis, D., and Ashe, H.L. (2011). Brat Promotes Stem Cell Differentiation via Control of a Bistable Switch that Restricts BMP Signaling. Dev. Cell *20*, 72–83.

Hoggatt, J., Kfoury, Y., and Scadden, D.T. (2016). Hematopoietic Stem Cell Niche in Health and Disease. Annu. Rev. Pathol. Mech. Dis. *11*, 555–581.

Hsu, Y.-C., and Fuchs, E. (2012). A family business: stem cell progeny join the niche to regulate homeostasis. Nat. Rev. Mol. Cell Biol. *13*, 103–114.

Huang, H., and Kornberg, T.B. (2016). Cells must express components of the planar cell polarity system and extracellular matrix to support cytonemes. Elife *5*, 1–20.

Inaba, M., Buszczak, M., and Yamashita, Y.M. (2015). Nanotubes mediate niche-stem-cell signalling in the Drosophila testis. Nature *523*, 329–332.

Kai, T., and Spradling, A. (2004). Differentiating germ cells can revert into functional stem cells in Drosophila melanogaster ovaries. Nature *428*, 564–569.

King, F.J., and Lin, H. (1999). Somatic signaling mediated by fs(1)Yb is essential for germline stem cell maintenance during Drosophila oogenesis. Development *126*, 1833–1844.

Lamaze, C., Fujimoto, L.M., Yin, H.L., and Schmid, S.L. (1997). The Actin Cytoskeleton Is Required for Receptor-mediated. J. Biol. Chem. *272*, 20332–20335.

Laurençon, A., Dubruille, R., Efimenko, E., Grenier, G., Bissett, R., Cortier, E., Rolland, V., Swoboda, P., and Durand, B. (2007). Identification of novel regulatory factor X (RFX) target genes by comparative genomics in Drosophila species. Genome Biol. *8*, R195.

Li, H., and Jasper, H. (2016). Gastrointestinal stem cells in health and disease: from flies to humans. Dis. Model. Mech. *9*, 487–499.

Lin, H., and Spradling, A.C. (1993). Germline stem cell division and egg chamber development in transplanted Drosophila germaria. Dev. Biol. *159*, 140–152.

Lu, W., Casanueva, M.O., Mahowald, A.P., Kato, M., Lauterbach, D., and Ferguson, E.L. (2012). Niche-associated activation of rac promotes the asymmetric division of Drosophila female germline stem cells. PLoS Biol. *10*, 10.

Mashinchian, O., Pisconti, A., Le Moal, E., and Bentzinger, C.F. (2018). The Muscle Stem Cell Niche in Health and Disease (Elsevier Inc.).

Michel, M., Raabe, I., Kupinski, A.P., Pérez-Palencia, R., and Bökel, C. (2011). Local BMP receptor activation at adherens junctions in the Drosophila germline stem cell niche. Nat. Commun. *2*, 412–415.

Norman, M., Vuilleumier, R., Springhorn, A., Gawlik, J., and Pyrowolakis, G. (2016). Pentagone internalises glypicans to fine-tune multiple signalling pathways. Elife *5*, 1–20.

Peck, B.C.E., Shanahan, M.T., Singh, A.P., and Sethupathy, P. (2017). Gut Microbial Influences on the Mammalian Intestinal Stem Cell Niche. Stem Cells Int. *2017*, 1–17.

Pedersen, L.B., Mogensen, J.B., and Christensen, S.T. (2016). Endocytic Control of Cellular Signaling at the Primary Cilium. Trends Biochem. Sci. *41*, 784–797.

Roy, S., Huang, H., Liu, S., and Kornberg, T.B. (2014). Cytoneme-mediated contact-dependent transport of the Drosophila decapentaplegic signaling protein. Science (80-.). *343*.

Sanchez, C.G., Teixeira, F.K., Czech, B., Preall, J.B., Zamparini, A.L., Seifert, J.R.K., Malone, C.D., Hannon, G.J., and Lehmann, R. (2016). Regulation of Ribosome Biogenesis and Protein Synthesis Controls Germline Stem Cell Differentiation. Cell Stem Cell *18*, 276–290.

Sano, H., Nakamura, A., and Kobayashi, S. (2002). Identification of a transcriptional regulatory region for germline-specific expression of vasa gene in Drosophila melanogaster. Mech. Dev. *112*, 129–139.

Shimmi, O., Umulis, D., Othmer, H., and O'Connor, M.B. (2005). Facilitated transport of a Dpp/Scw heterodimer by Sog/Tsg leads to robust patterning of the Drosophila blastoderm embryo. Cell *120*, 873–886.

Snyder, J.C., Rochelle, L.K., Marion, S., Lyerly, H.K., Barak, L.S., and Caron, M.G. (2015). Lgr4 and Lgr5 drive the formation of long actin-rich cytoneme-like membrane protrusions. J. Cell Sci. *128*, 1230–1240.

Song, X., Zhu, C.-H., Doan, C., and Xie, T. (2002). Germline stem cells anchored by adherens junctions in the Drosophila ovary niches. Science *296*, 1855–1857.

Song, X., Wong, M.D., Kawase, E., Xi, R., Ding, B.C., McCarthy, J.J., and Xie, T. (2004). Bmp signals from niche cells directly repress transcription of a differentiation-promoting gene, bag of marbles, in germline stem cells in the Drosophila ovary. Development *131*, 1353–1364.

Tanimoto, H., Itoh, S., Ten Dijke, P., and Tabata, T. (2000). Hedgehog creates a gradient of DPP activity

in Drosophila wing imaginal discs. Mol. Cell *5*, 59–71.

Teixeira, F.K., Sanchez, C.G., Hurd, T.R., Seifert, J.R.K., Czech, B., Preall, J.B., Hannon, G.J., and Lehmann, R. (2015). ATP synthase promotes germ cell differentiation independent of oxidative phosphorylation. Nat. Cell Biol. *17*, 689–696.

Teleman, A.A., and Cohen, S.M. (2000). Dpp gradient formation in the drosophila wing imaginal disc. Cell *103*, 971–980.

Wilcockson, S.G., Sutcliffe, C., and Ashe, H.L. (2017). Control of signaling molecule range during developmental patterning. Cell. Mol. Life Sci. *74*, 1937–1956.

Xia, L., Zheng, X., Zheng, W., Zhang, G., Wang, H., Tao, Y., and Chen, D. (2012). The niche-dependent feedback loop generates a BMP activity gradient to determine the germline stem cell fate. Curr. Biol. *22*, 515–521.

Xie, T., and Spradling, A. (2000). A Niche Maintaining Germ Line Stem Cells in the Drosophila Ovary. Science *290*, 328–330.

Xie, T., and Spradling, A.C. (1998). decapentaplegic is essential for the maintenance and division of germline stem cells in the Drosophila ovary. Cell *94*, 251–260.

Zhang, Q., Shalaby, N.A., and Buszczak, M. (2014). Changes in rRNA Transcription Influence Proliferation and Cell Fate-Science2014.pdf. *343*, 298–302.

METHODS

Flies were grown at 25°C using standard procedures, unless otherwise stated. The following fly lines were used in this study; *vasa.eGFP.HA* (Kyoto Stock Center), *bam.GFP* (Chen and McKearin, 2003), *UASp-tkv^{QD}* (Tanimoto et al., 2000), CRISPR knock-in *dpp^{mCh}* and *tkv^{mCh}* flies were a gift from R. Hatori and T. Kornberg (unpublished), *dally^{mCh}* (Norman et al., 2016), *BamΔ27::TIPF* (Michel et al., 2011), *dpp^{HA}* (Shimmi et al., 2005). The following were obtained from Bloomington Stock Center; *dpp^{hr92}*, *tkv^{7}, mad$^{1-2}$*, *med^{13}*, *UAS-dpp^{GFP}, bab1-Gal4, tub-Gal80^{ts}, nos-Gal4::VP16*, *UASp-bam^{shRNA}*, *UASp-eGFP.αTubulin84B*, *UASp-Actin42A.eGFP*, *UASp-Actin5c.mRFP*, *UASp-LifeAct.eGFP*, *UASp-FTractin.dTomato* and *UASp-shRNA* lines. For RNAi, flies were moved to 29°C for 1 week post-eclosion before dissection to enhance the knockdown. For temporal control of *dia^{shRNA}* or *Gal80^{ts}* flies were raised at 18°C and then either kept at 18°C or moved to 25°C or 29°C for 3 days before dissection (See text).

RNA-seq

For each RNA sample 300-400 ovary pairs were dissected from 3-5 day old flies. Ovaries were dissected into 1x PBS on ice and incubated in 5 mg/ml collagenase IV in PBS (Worthington Biochemicals) at RT for 45 min to dissociate the tissue. Cells were washed in PBS and filtered through a 40 µm nylon mesh to remove debris before fluorescence-activated cell sorting (FACS) based on the expression of *vasa.GFP* or *bam.GFP* using a FACSAria™ Fusion cell sorter (Diva 8 Software; BD

Biosciences). Cells were sorted into 1x PBS on ice and RNA was isolated using TRIzol (Invitrogen). Total RNA was processed and sequenced by the Genomic Technologies Core Facility (University of Manchester) on the Illumina Genome Analyser II. Reads were mapped to the *Drosophila* genome (dm3) and gene counts were analysed using HTSeq. DESeq2 was used to calculate differential expression between genotypes and differentially expressed genes were determined to be at least 2-fold more highly expressed than the other genotype with a $p < 0.05$. GO term analysis was carried out using the Gene Ontology Consortium with Fisher's Exact with FDR multiple test correction.

***ex vivo* live imaging**

For live imaging 3-5 day old flies were dissected in Schneider's Insect Media (Thermofisher) supplemented with 10% Fetal Bovine Serum (FBS) (Thermofisher), 1% (w/v) penicillin/streptavidin (Sigma) and individual ovarioles were separated and the overlying muscle removed to reduce movement during imaging. Ovarioles were mounted on a 35mm glass bottom tissue culture dish (World Precision Instruments) in a drop of Schneider's Insect Media (10% FBS, 1% pen/strep) supplemented with 10 mg/ml fibrinogen (Millipore) which is spread across the glass bottom well before adding thrombin (10 U/ml GE Healthcare Lifesciences) to clot the fibrinogen. Schneider's Insect Media (10% FBS, 1% pen/strep) supplemented with 200 mg/ml Human insulin (Sigma) was added and ovarioles were maintained at room temperature for 2-3 hours.

Germaria were imaged using a Leica TCS SP8 AOBS inverted microscope using a HC PL APO CS2 motCORR 63x/1.2 water objective with 5-6x confocal zoom with a pinhole size of 1 AU, scan speed 400 Hz unidirectional, format 512 x 512, 2x line averaging, with 10-20 *z*-stacks taken at 0.75 µm intervals every 30-60 seconds. Imaging was carried out at room temperature for 1-3 hours and images were subsequently analysed using Fiji. For later analysis, a brightfield image was taken to localise the GSCs and niche.

Immunofluorescence imaging

Ovaries were fixed in 4% formaldehyde in PBT (1x PBS, 0.1% Triton X-100) for 15 minutes, washed three times for 15 minutes in PBT and blocked in 10% Bovine serum albumin (BSA) in PBT for 30 minutes before overnight incubation with primary antibodies in 10% BSA in PBT at 4°C. Ovaries were then washed 4 times in PBT over an hour and incubated with secondary antibodies for 2 hours at room temperature. They were then washed twice for 15 minutes in PBT and once for 15 minutes in PBS before mounting in Prolong Gold Antifade with DAPI (Invitrogen). For phalloidin staining, ovaries were incubated for 30 minutes (during the second PBT wash before mounting) and wash twice for 15 minutes with PBT before mounting. Fixed germaria were imaged using a Leica TCS SP5 AOBS inverted microscope using an HCX PL APO 63x/1.4 oil objective or PL APO 100x/1.4 oil objective.

For visualising microtubule projections, flies were fixed in PEM buffer (80 mM PIPES (Sigma), 1 mM $MgCl_2$ (Sigma), 5 mM EGTA (Sigma), pH 7.4) with 4% formaldehyde and 2 µM paclitaxel (Sigma) for 30 minutes and rinsed twice in PEM buffer and washed in 3 times for 15 minutes PBT (1x PBS, 0.1% Triton X-100) before blocking in 10% BSA in PBT for 30 minutes. Protocol was followed as outline above.

For visualising extracellular proteins only, ovaries were fixed in PEM buffer with 4% formaldehyde for 15 minutes and washed in PEM three times for 15 minutes. Protocol was followed as outline above substituting PBS and PBT for PEM buffer (with no detergent). Antibodies were used higher concentrations; Rt anti-DCAD2 (DSHB, 1:10), Rb anti-mCherry (ab183628, 1:50), Ms anti-HA 12CA5 (Roche, 1:50) and Rb anti-GFP (ab6556, 1:50). Ovaries were mounted in Prolong Gold Antifade with DAPI.

To visualise endogenous TIPF and mCherry fluorescence, ovaries were fixed in PEM buffer with 4% formaldehyde for 15 minutes, before washing with PEM three times for 15 minutes. Ovaries were mounted in Prolong Gold Antifade and immediately imaged.

For *ex vivo* treatment with actin and microtubule depolymerising drugs, 5 per treatment were dissected in PBS and collected in Schneider's Insect Media (10% FBS, 1% pen/strep). Ovaries were incubated with either the vehicle DMSO (Sigma), 2µM cytochalasin D (Sigma), 10µM nocodazole (Sigma) for 30 mins or 90 mins at 25°C. Ovaries were rinsed with PBS and fixed. Protocol was follows as previous described.

Antibodies used include; Rb anti-GFP (ab6556, 1:250), Chk anti-GFP (ab13970, 1:500), Rb anti-mCherry (ab183628, 1:500), Ms anti-RFP (ab65856, 1:250), Ms anti-αSpectrin 3A9 (DSHB, 1:50), Rt anti-DCAD2 (DSHB, 1:50), Ms anti-Futsch 22C10 (DSHB, 1:50) Rb anti-pSmad3 (ab52903, 1:500), Rt anti-αTubulin [YL1/2] (ab6160, 1:200), Ms anti-acetylated αTubulin [6-11b-1 (ab24610, 1:500), anti-γTubulin (Sigma GTU-88, 1:250), Rb anti-Vasa (Santa Cruz, 1:500). Secondary antibodies used were Alexa Fluor 488 Donkey anti-Ms, Alexa Fluor 488 Goat anti-Chk, Alexa Fluor 555 Donkey anti-Ms, Alexa Fluor 597 Donkey anti-Rt, Alexa Fluor 647 Donkey anti-Rt, Alexa Fluor 647 Donkey anti-Rb and Alex Fluor 488 Phalloidin (Thermofisher).

Quantification and Statistical Analysis

Cytosensor length was measured using the line tool in Fiji to measure from the tip of the projection to the base. Thickness was measured at the base.

Live images were maximum projected to analyse actin-based projections and analysed in Fiji. Length was measured using the line tool to measure from the tip of the projection to the base at the point at which it achieves its maximum length. Extension speed was measured as the time taken from the point of projection nucleation and reaching maximum length. Retraction speed is defined as the time it takes a projection to completely collapse after reaching its maximum length. Lifetime is measured as the total amount of time the projection is visible for. The two-dimensional angle of nucleation was measured using the angle tool in Fiji to draw a line from the centre of the niche, determined from a brightfield view of the germarium, to the centre of the stem cell or cystoblast.

To measure pMad fluorescence, z-stacks (sum of slices) were generated at 0.75µm intervals of all 10-12 slices incorporating individual GSCs. Using the draw tool in Fiji, a circle encompassing the GSC was drawn and the integrated fluorescence density (IFD) was taken and background subtracted (IFD -

(average mean intensity of background x area of the region sampled). All results were then normalised to controls.

Quantification of germ cell numbers was carried out using spectrosome staining. GSCs were classed as germ cells localised at the anterior tip of the germarium in contact with the niche and containing an anteriorly anchored spectrosome. Early germ cell quantification included GSCs and any additional round spectrosome containing cells.

To count TIPF puncta, a brightfield image of the germarium was used to locate the niche.

Statistical comparisons were performed using using two-tailed Student's t-tests, one-way ANOVA with multiple comparisons or paired t-test (Fig. 6C) using GraphPad Prism.

FIGURE LEGENDS

Figure 1. GSCs up-regulate MT-associated factors and extend GSC cytoskeletal projections into the niche.

(A) Cartoon depicting the structure of the germarium and GSC niche.

(B) Immunostaining of a germarium with germline-specific expression of constitutively active Tkv (Tkv^{QD}) reveals tumours of $pMad^{+}$ GSC-like cells.

(C) Expression of Bam-GFP marks differentiating daughter CBs.

(D) Expression of Vasa-GFP marks all germ cells.

(E) Differential expression analysis of RNA enriched in tkv^{QD} (magenta) and *bam.GFP* (green) expressing cells. Pie chart shows number of significantly enriched genes for each cell type (log_2Fold change>0.5, p<0.05).

(F) GO term analysis results showing biological processes enriched in in tkv^{QD} (magenta) and *bam.GFP* (green) expressing cells.

(G) Germline expression of bam^{shRNA} generates tumours of $pMad^{-}$ GSC-like cells.

(H) and (I), as in (E) and (F) comparing tkv^{QD} (magenta) and bam^{shRNA} (light pink).

(J-K) Immunofluorescence staining of germaria with germline ***eGFP.αTub*** expression. GSCs marked by the spectrosome visualised with anti-αSpectrin, E-cadherin outlines the CpCs (*). Dashed line marks a GSC and bracket marks MT-rich projection. (K) Futsch localises to MT-rich projections.

(L) GSCs form different actin-rich projections. Immunofluorescence staining of germaria with germline expression of ***eGFP.αTub*** and *Act.mRFP*. A GSC extends one MT- and actin-rich projection (green arrowhead) and one actin-based filopodium (magenta arrowhead).

(M) Percentage of GSCs forming projections after 30min *ex vivo* treatment of *nos-Gal4>Act42A.GFP or eGFP.αTub* ovaries with DMSO (control), 2µM cytochalasin D or 10µM nocodazole. Mean and SD from n>100 GSCs. ns, not significant; *, p<0.0001.

Scale bar = 10µm (A-G) or 5µm (J-L) or 1µm (insets J-L). See also Figure S1.

Figure 2. GSC projections are dynamic and all early germ cells form actin-rich projections

(A) Stills from Movie 1 showing a cytocensor labelled with ***eGFP.αTub***. Time is in minutes.

(B) Stills from Movie 2 showing F-actin with *LifeAct.GFP* in GSCs (false coloured magenta), CBs (green) and 2- or 4-cell cysts (blue). Insets focus in on the niche (*) and niche-directed actin-rich projections (brackets).

(C) same as (B) showing stills from Movie 3. (i, top) First 2 slices of a maximum projection showing a broad lamellipodia-like projection (F-actin between brackets) depicted in cartoon form on the left and axes denote position within the maximum projection. (i, middle) 2 slices in the middle of the maximum projection reveal two niche cells that the lamellipodia projects over. (i, bottom) *xz*-plane view showing the filopodium from the side, extending into the *z*-plane. (ii) All early germ cells form multiple actin-rich projections (arrowheads).

(D) Cartoon and scatter plot showing the angle of actin filopodia nucleation point relative to the centre of the niche (0°). 'Niche-directed' filopodia are defines as those forming at an angle <45° to the centre of the niche. The rest are 'lateral projections'. (n=100 GSC projections and n=50 CB projections)

(E-I) Box and whisker plots comparing the length (E), lifetime (G), extension (H) and retraction speed (I) of actin projections from the following classes; $GSC^{<45°}$ (light pink), $GSC^{>45}$ (magenta), CBs (green) and 2-cell cysts (blue). Median, 25th and 75th percentile and whiskers show minima and maxima. n=46-50 projections from n>8 cells. *, p<0.0001.

Scale bar = 2µm (A) or 5µm (B-C). See also Figure S2.

Figure 3. Cytocensors are regulated by stem cell enriched MT-associated factors and form in response to Dpp signalling.

(A) Germline-specific *shRNA e*xpression phenotypes for the indicated MT-associated factors and actin regulators disrupts projection formation.

(B-C) Box and whisker plots of cytocensor length (B) and thickness (C) following knock down of the expression of MT-associated factors (blue), ciliogenesis factors (green) and actin regulators (red). Median, 25th and 75th percentile and whiskers show minima and maxima. n=46-50 projections from n>8 cells. *, p<0.05; **, p<0.001, ***, p<0.0001.

(D) Bar chart showing number of cytocensors formed per GSC for knockdown of factors as in (B-C). Mean and SEM. *, p<0.05, ***, p<0.0001.

(E-H) Heterozygous mutants for Dpp signalling pathway components, $dpp^{hr92/+}$, $tkv^{7/+}$, $med^{13/+}$ and $mad^{1-2/+}$, typically form abnormal cytocensor compared to controls. Decreased Dpp signalling reduces projection formation (F) while those that are formed are abnormal in length (H) and/or thickness (G). Statistics as in (B-D). #, significant difference in variance p<0.01 F-test

(*) Niche cells; brackets show lengths and thickness of projections. Scale bars = 2µm. See also Figure S3.

Figure 4. Niche cells create a Dally-Dpp reservoir where GSC Tkv activation occurs

(A-B) Extracellular immunostaining of E-cadherin and endogenous mCherry-tagged Dpp (A) or Dally (B). Line shows where the plot of fluorescence intensity (Ai-Bi) was taken from anterior to interface (A to I) through the centre of the niche (*). E-cadherin defines the niche cell boundaries.

(C) Anterior to interface ratio of fluorescence intensity of Dpp^{mCh} is plotted. *Dally^{shRNA}* or over-expression is induced at 29°C and compared to non-induced at 18°C. Line shows mean. n=20 niche cells, *, p<0.01; **, p<0.0001.

(D) Endogenous fluorescence of Dally^{mCh} and germline expressed TIPF reporter (*BamΔ27::TIPF*) around the niche (D') Percentage co-occurrence of TIPF and Dally^{mCh} puncta. Mean and SD.

(E) Cartoon model showing that GSCs present Tkv on projections to access a Dally-Dpp reservoir.

(F) Endogenous fluorescence of TIPF reporter with *Dally^{shRNA}* or over-expression in inverted black and white for clarity (as in C).

(G) Plot showing the number of TIPF puncta per germaria in (F). Line shows mean, n=20 germaria, *, p<0.01, **, p<0.001.

Dashed lines (D and F) outline the niche. Scale bar = 2µm. See also Figure S4

Figure 5. Tkv is trafficked onto GSC projections which act as signalling platforms

(A) Stills showing F-actin labelled with *LifeAct.GFP* and endogenous mCherry-tagged Tkv showing an actin-rich projection (bracket) and the accumulation of Tkv^{mCh} at the base (magenta arrowhead) before accumulation on the projection.

(B) Stills showing the trafficking of Tkv^{mCh} puncta (magenta arrowhead) on a cytosensor labelled with *eGFP.αTub.*

(C) Stills showing Dpp^{mCh} puncta (magenta arrowhead) statically associated with a cytosensor labelled with *eGFP.αTub.*

(D) Stills showing Tkv activation (TIPF fluorescence, yellow arrowhead) occurring on an actin-rich projection and accumulated active Tkv at the base of the projection (open yellow arrowhead).

Projections are outline by dashed lines. (*) niche cells. Scale bars = 1µm. See also Figure S5.

Figure 6. Knockdown of *dia* expression causes dysregulation actin projections and Dpp signalling

(A) Germline-specific *dia^{shRNA}* expression phenotypes comparing flies raised at 18°C for 3 days (inhibiting shRNA expression) to those raised at 25°C for 3 days (inducing shRNA expression). pMad staining reports the Dpp signalling response. Early germ cells are marked by the presence of the spectrosome labelled by anti-αSpectrin.

(B) Histogram showing quantification of GSC numbers in (A) n=50 germaria for control, n≥142 for *dia^{shRNA}*.

(C) Comparison of pMad fluorescence of germaria described in (A). GSC1 is the cell with the highest pMad and GSC2 has the lowest. n>15 germaria *, p<0.001.

(D) Ratio of pMad levels from (C). *, p<0.001.

(E) Percentage of *dia^{shRNA}* expressing GSCs that form actin-rich projections labelled with LifeAct.GFP. n>100 GSCs, *, p<0.0001

(F) A single polyploid *dia^{shRNA}* expressing GSC that has occupied an entire niche.

(G-H) Stills from movies showing actin projections labelled with LifeAct.GFP in wildtype (G) and *dia*^{shRNA} expressing germ cells. Brackets label niche-directed projections and arrow heads label lateral projections. GSC (false coloured magenta), CB (green) and 2 or 4-cell cysts (blue).
Niche cells (*). Scale bars = 5µm (A and F) or 2µm (G and H).

Figure 7. Cytocensors attenuate Dpp signalling to regulate GSC self-renewal and differentiation

(A) Endogenous TIPF fluorescence after 30 or 90 mins *ex vivo* drug treatment. (A') Scatter plot showing number of TIPF puncta per niche after treatment with either DMSO (n=24 each), 2µM cytochalasin D (n=28 and 12, respectively) or 10µM nocodazole (n=24 each). ns, not significant; *, p<0.05; **, p<0.001; ***, p<0.0001.

(B) Germline-specific *shRNA e*xpression phenotypes. pMad staining reports the Dpp signalling response. Early germ cells are marked by the presence of the spectrosome (open arrowhead) labelled by anti-αSpectrin.

(C) Histogram showing quantification of GSC numbers in (B) and differentiation phenotype. n≥100 germaria.

(D) Comparison of pMad fluorescence relative to control from (B). Median, 25th and 75th percentile and whiskers show minima and maxima. n≥15 cells; *, p<0.001.

(E) Model illustrating the role of actin projections in promoting Dpp signal transduction and cytocensors in modulating levels through signal suppression. See text for details.

Dashed lines in (A) outline the niche. Scale bar = 10µm (B) or 5µm (A).

Wilcockson et al. Figure 1

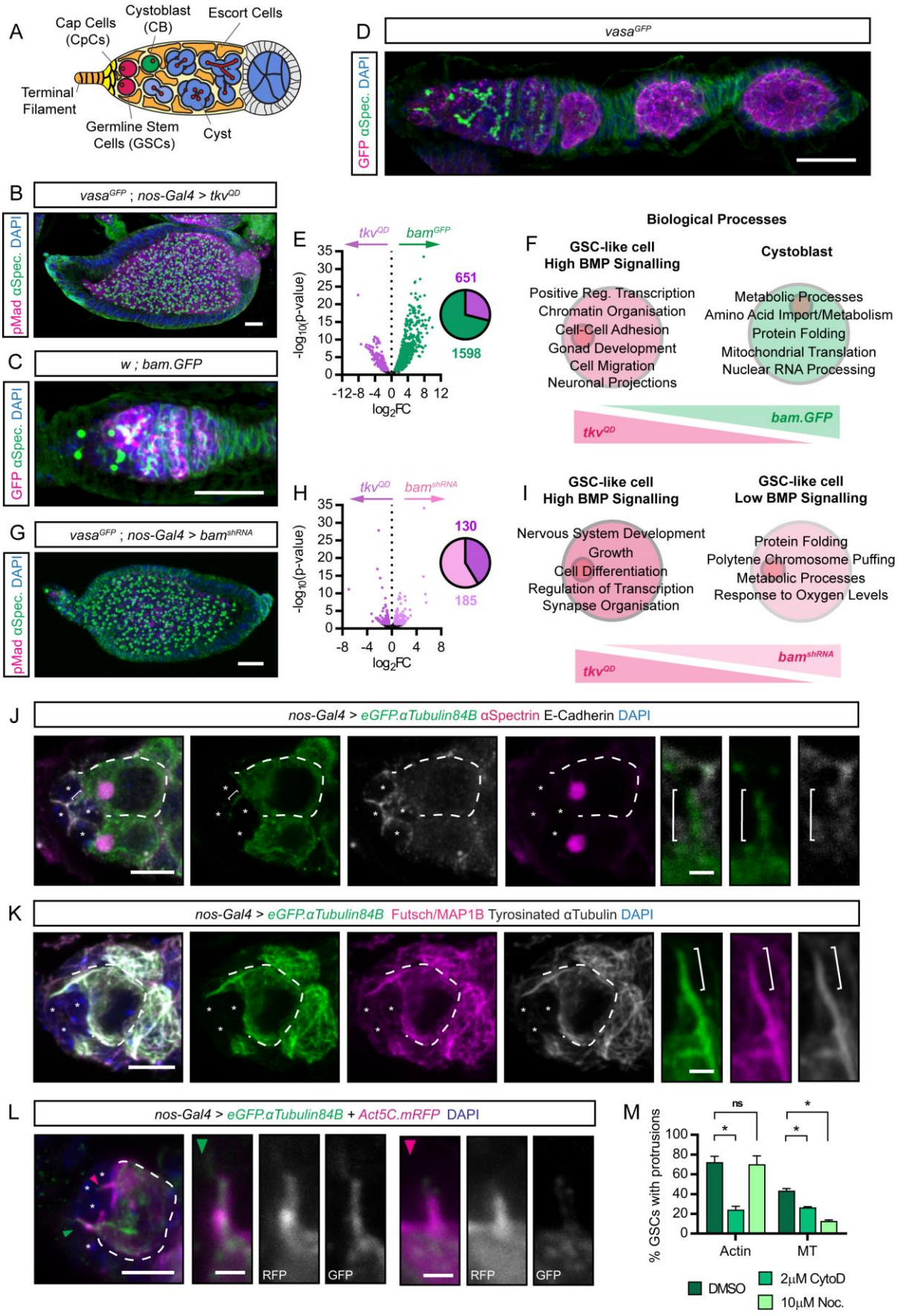

Wilcockson et al. Figure 2

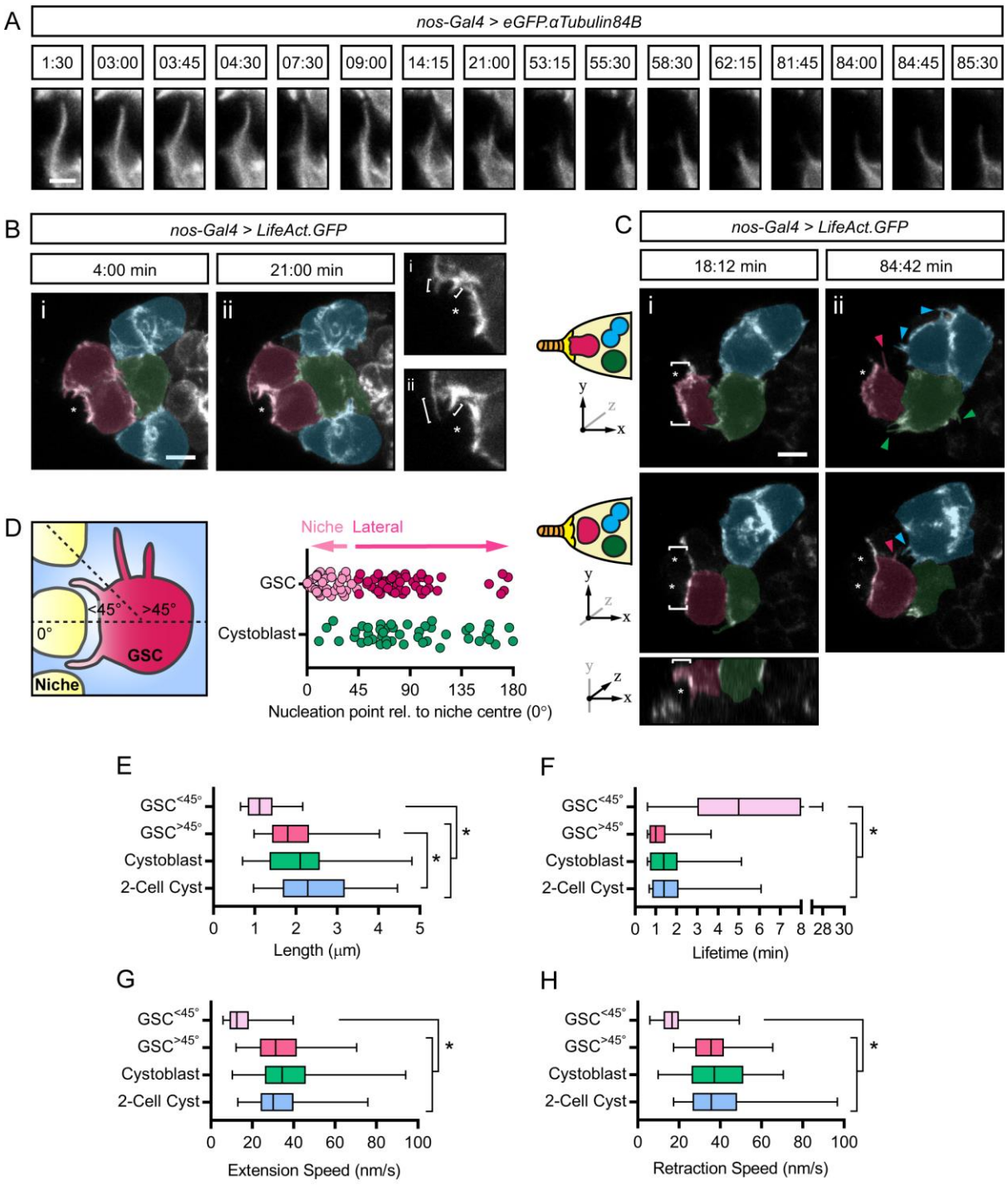

Wilcockson et al. Figure 3

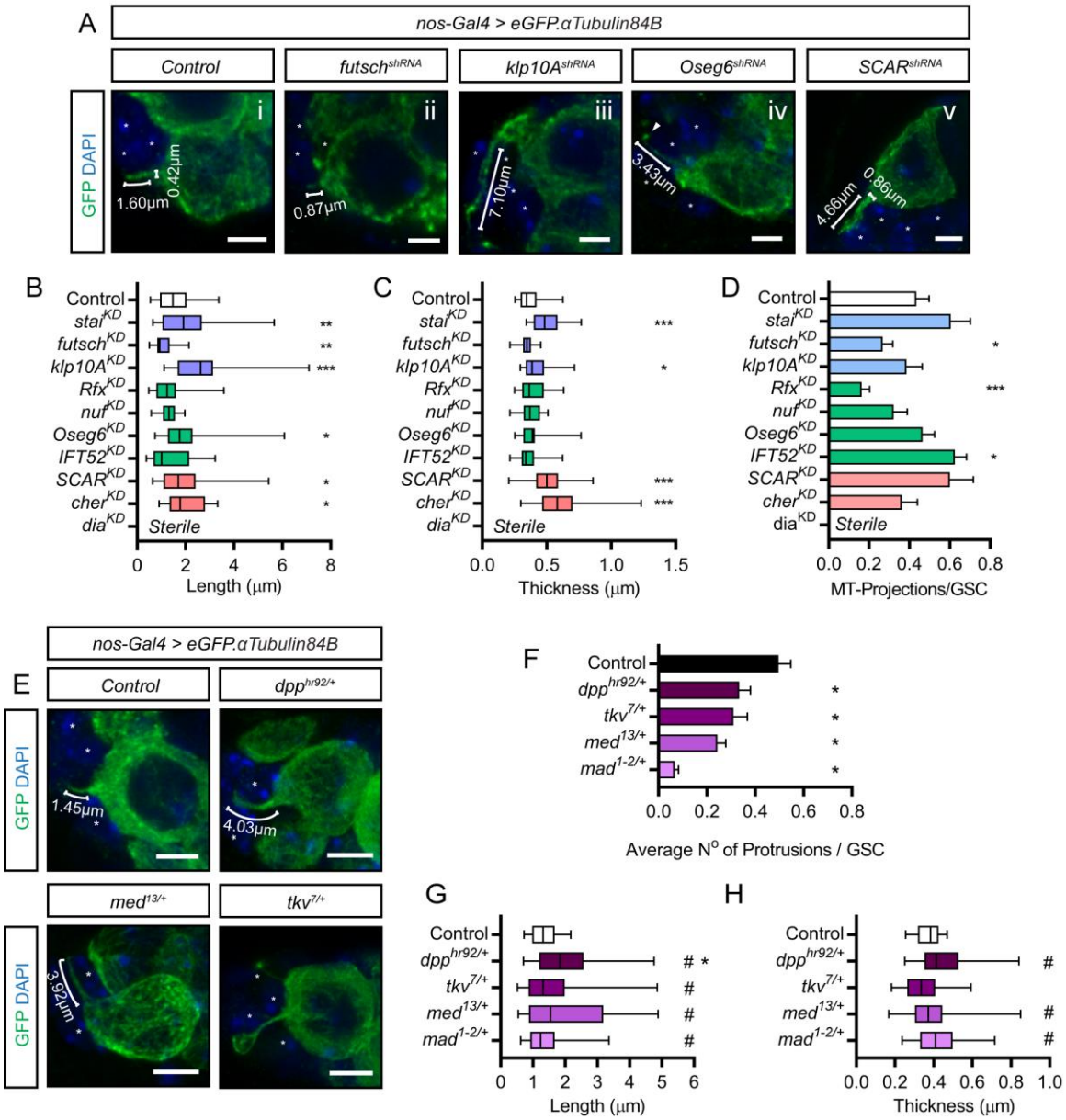

Wilcockson et al. Figure 4

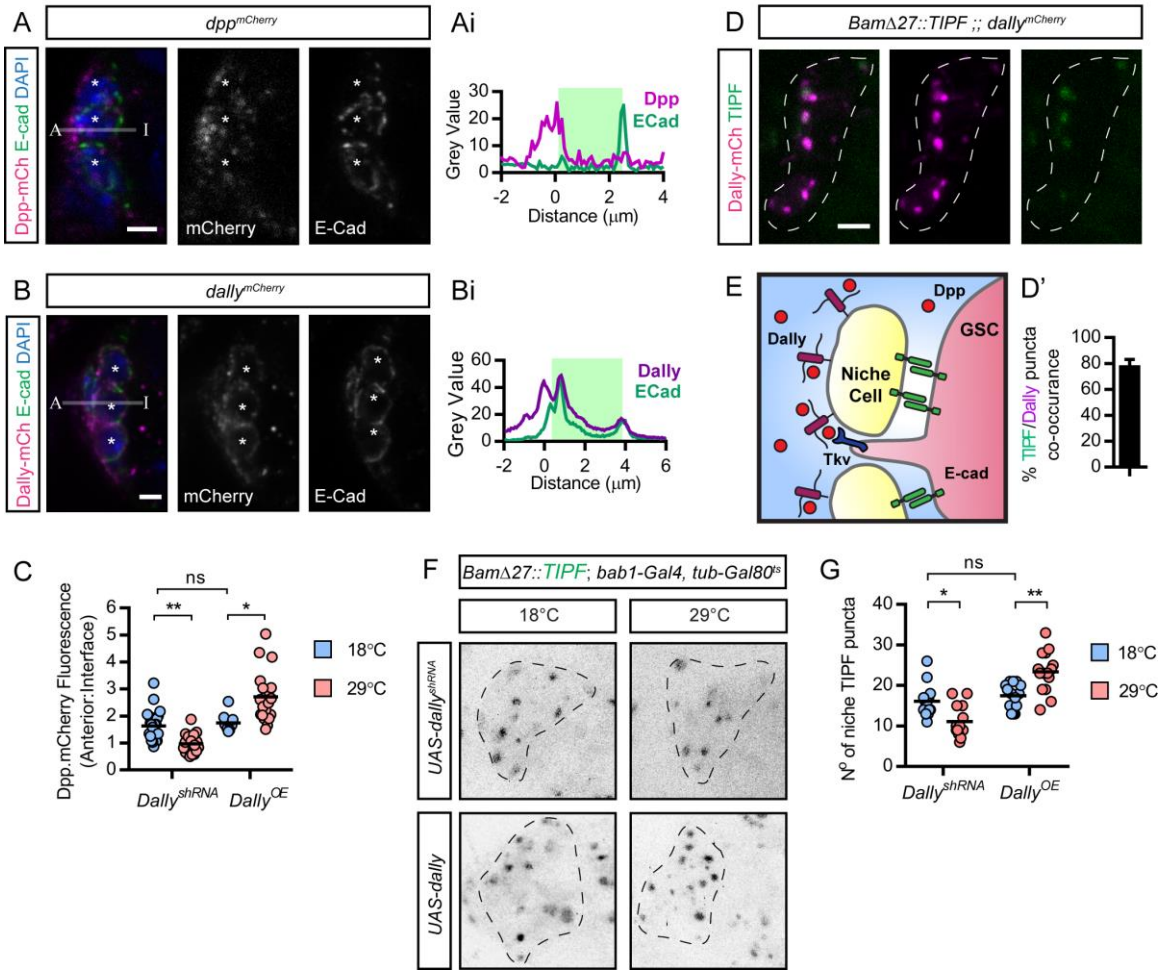

Wilcockson et al. Figure 5

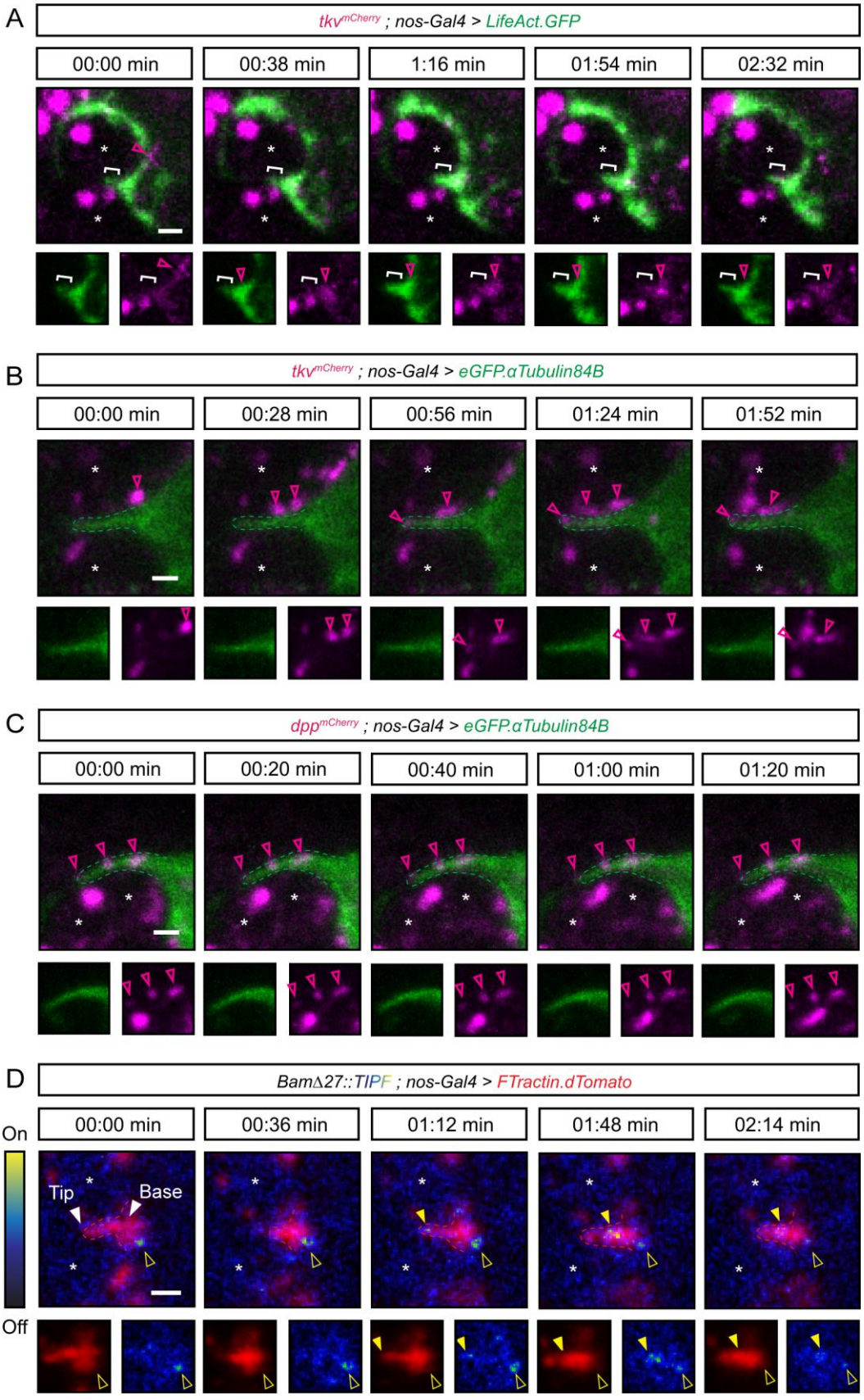

Wilcockson et al. Figure 6

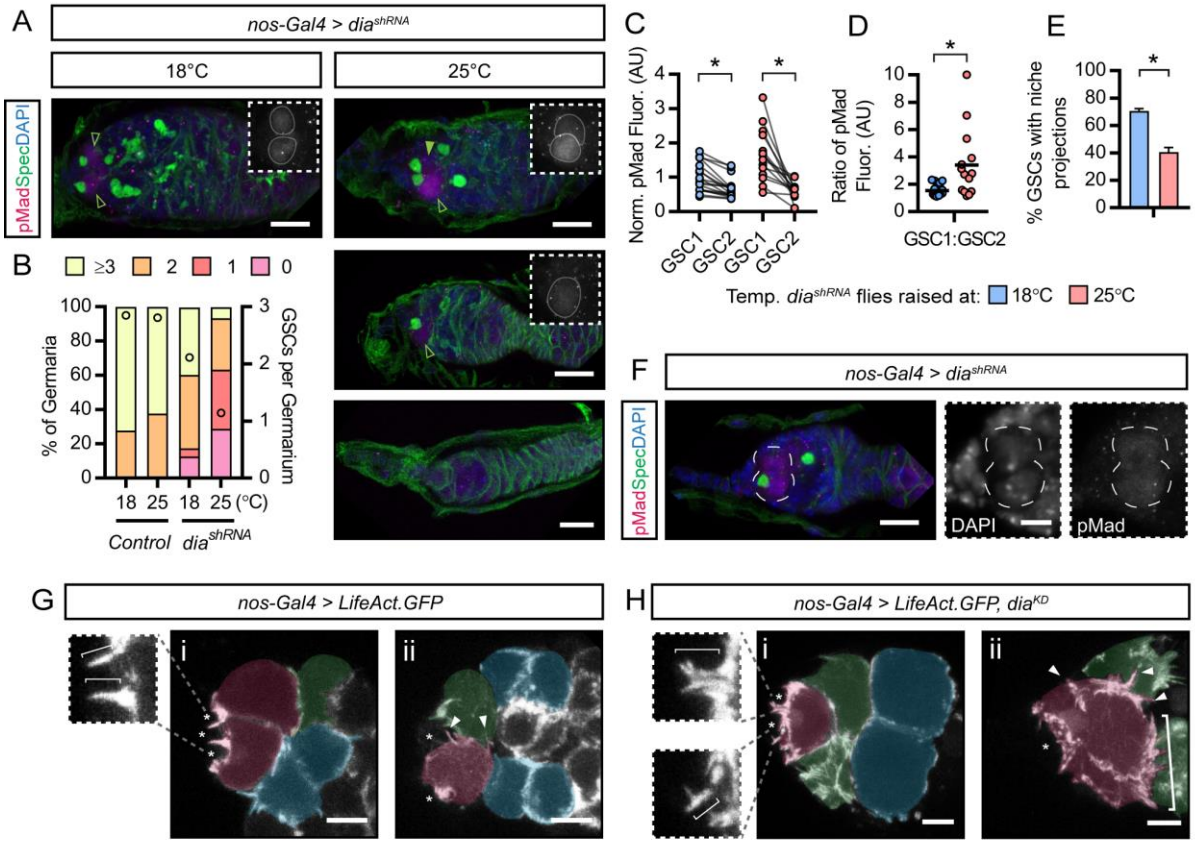

Wilcockson et al. Figure 7

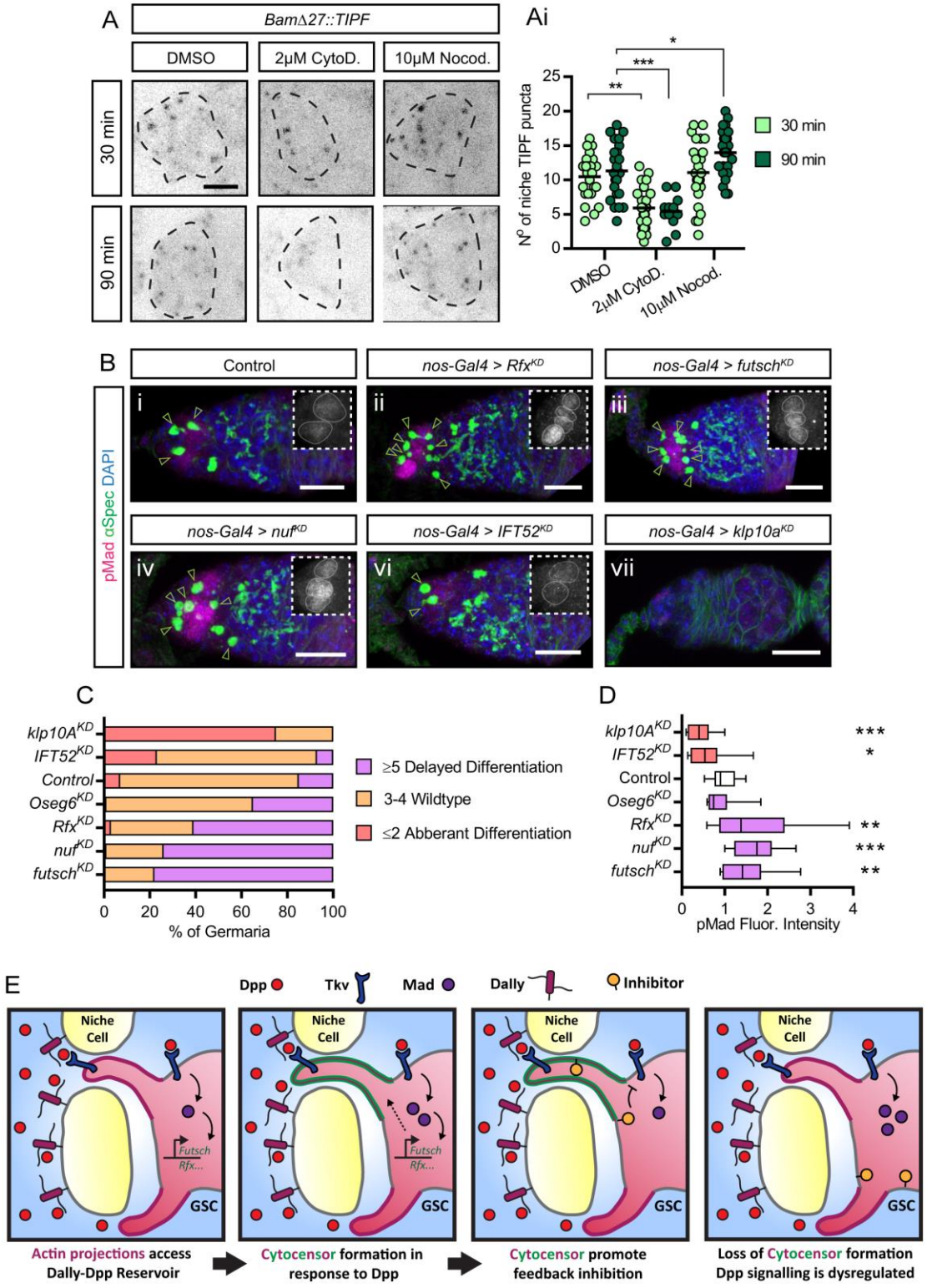

SUPPLEMENTAL INFORMATION

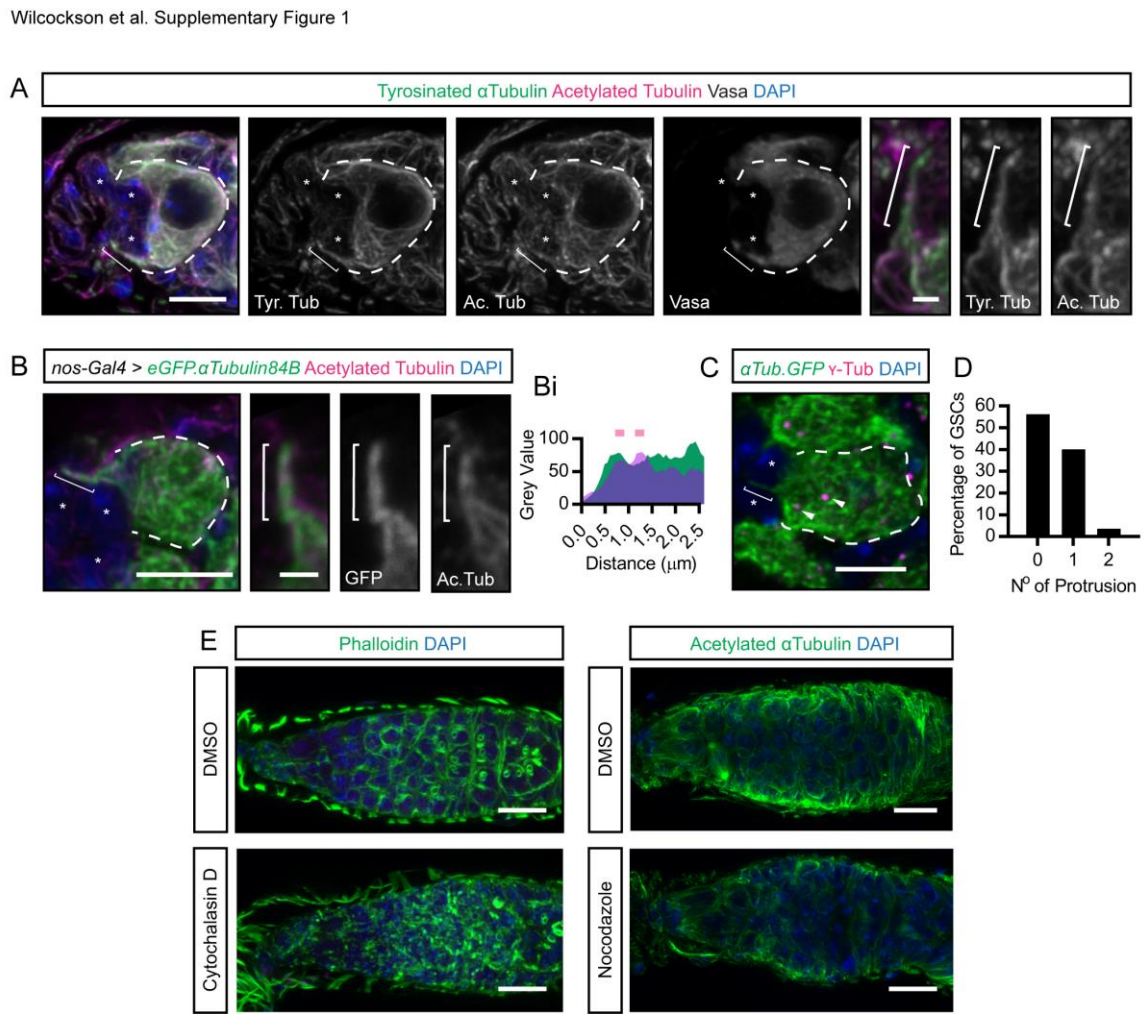

Figure S1. Composition of GSC projections. Refers to Figure 1

(A) Immunofluorescence stain of germaria MT network. GSCs marked by the Vasa expression (white). MTs are labelled by the stable MT marker, acetylated αTubulin, and the young dynamic MT marker, tyrosinated αTubulin.

(B) eGFP-αTub84B labelled MT-projection labelling acetylated MTs. (Bi) fluorescence intensity plot along the shaft of the MT-projection. Magenta lines denote highly acetylated regions.

(C) Centrosome localisation, labelled by γ-tubulin, relative to MT-projection.

(D) Frequency of MT-rich projection formation per GSC.

(E) Testing *ex vivo* drug treatment on germaria. A 30 min treatment with 2μM cytochalasin D leads to fragmentation of actin, stained with phalloidin, and the accumulation of cytoplasmic puncta. Similar treatment with 10μM nocodazole reduces acetylated tubulin levels.

Scale bar = 5μm (enlarged) or 1μm (insets) Niche cells (*). Dashed line marks a GSC and bracket marks MT-rich projection.

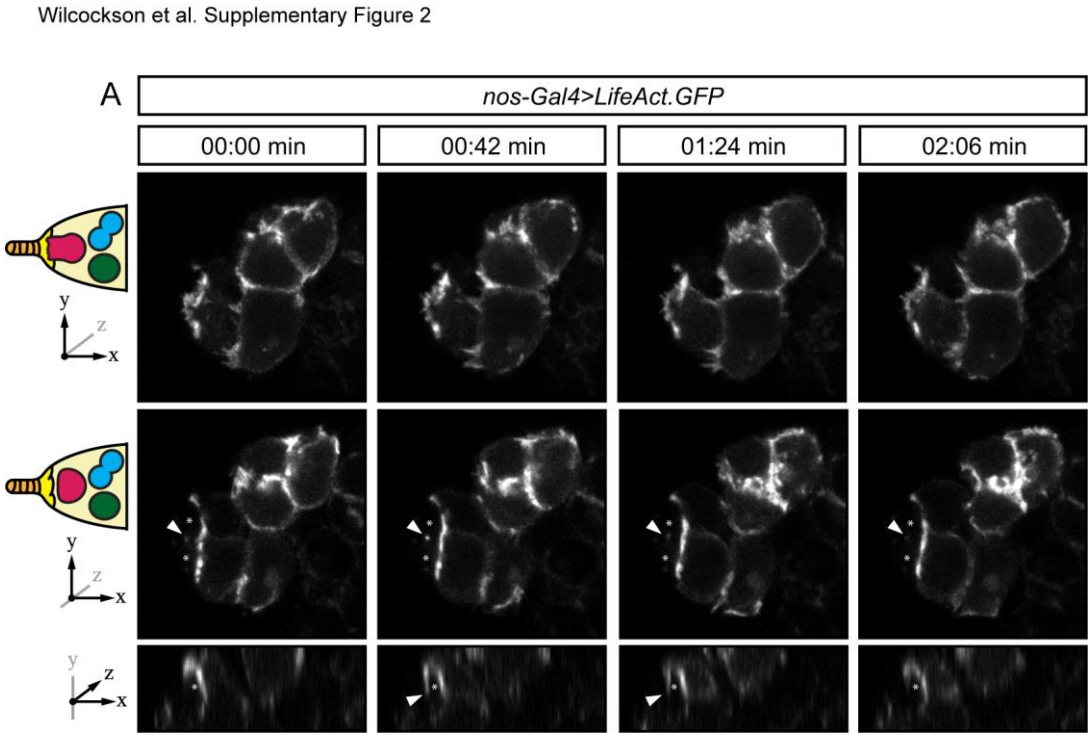

Figure S2. Filopodium extension from a lamellipodia allowing a stem cell to envelope a niche cell. Refers to Figure 2

(A) Stills from Movie 3 showing F-actin in GSCs. Top panels show first 2 slices of a maximum projection showing a broad lamellipodia-like projection depicted in cartoon form on the left and axes denote position within the maximum projection. Middle panels show 2 slices in the middle reveal two niche cells the lamellipodia projects over. Bottom panel shows *xz*-plane view. Arrowhead marks the bisected shaft (middle) or entire finger-like filpodium (bottom). Niche cells (*).

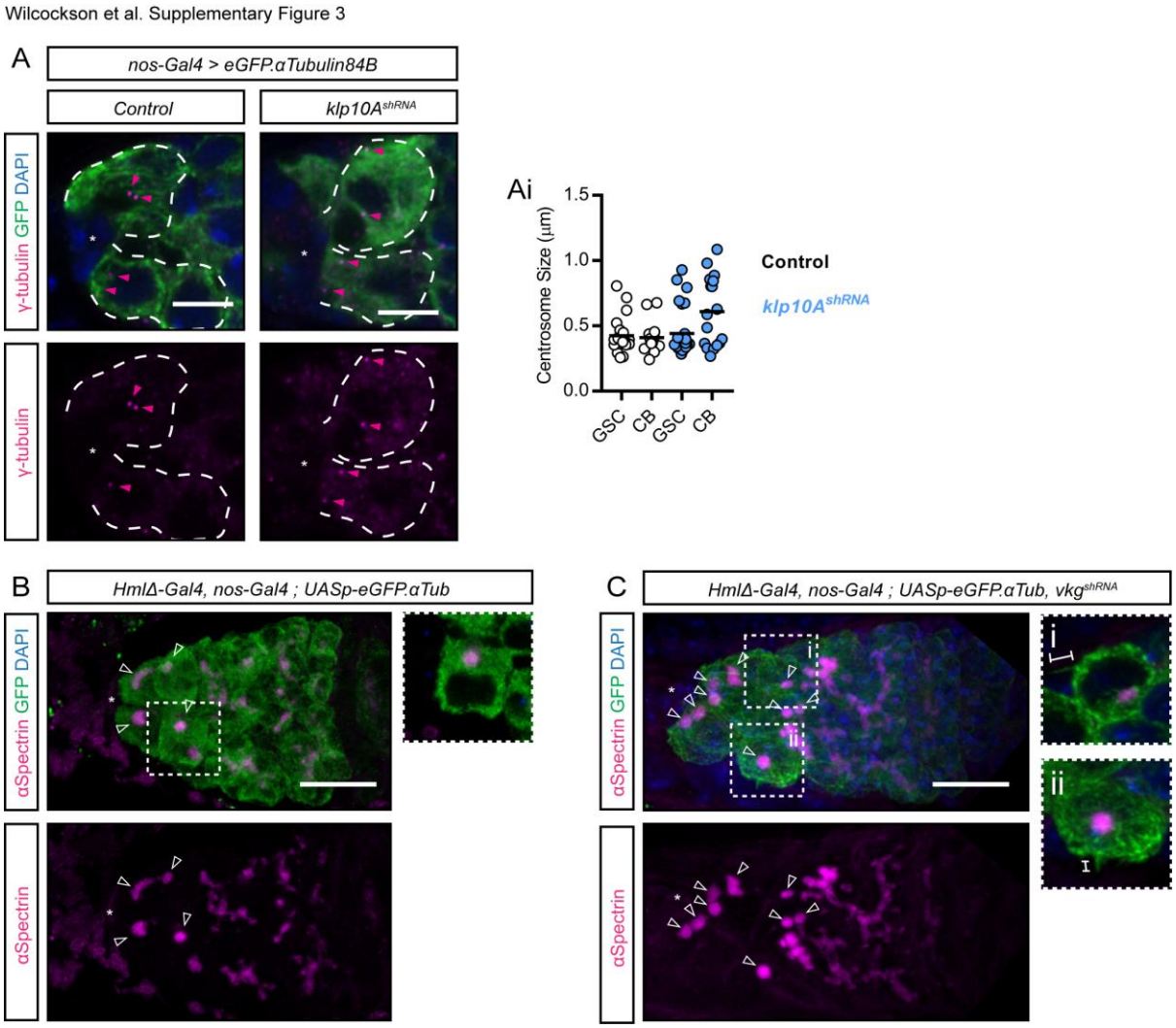

Figure S3. Ectopic Dpp signalling induces cytocensor formation. Refers to Figure 3

(A and Ai) Unlike in the male germline, *klp10A* knockdown has no effect on the GSC centrosome size (labelled with γ-tubulin).

(B and C) Germline and haemocyte specific expression of eGFP-αTub84B and RNAi-knockdown of *vkg* expression. (A) Control germaria have 3-4 early germ cells (arrowheads) and cells that exit the niche (inset) do not typically generate cytocensors. (B) Knockdown of *vkg* expression in larval haemocytes extends the range of Dpp in the germarium, leading to ectopic germ cell accumulation and cytocensor formation by cells that have exited the niche (inset).

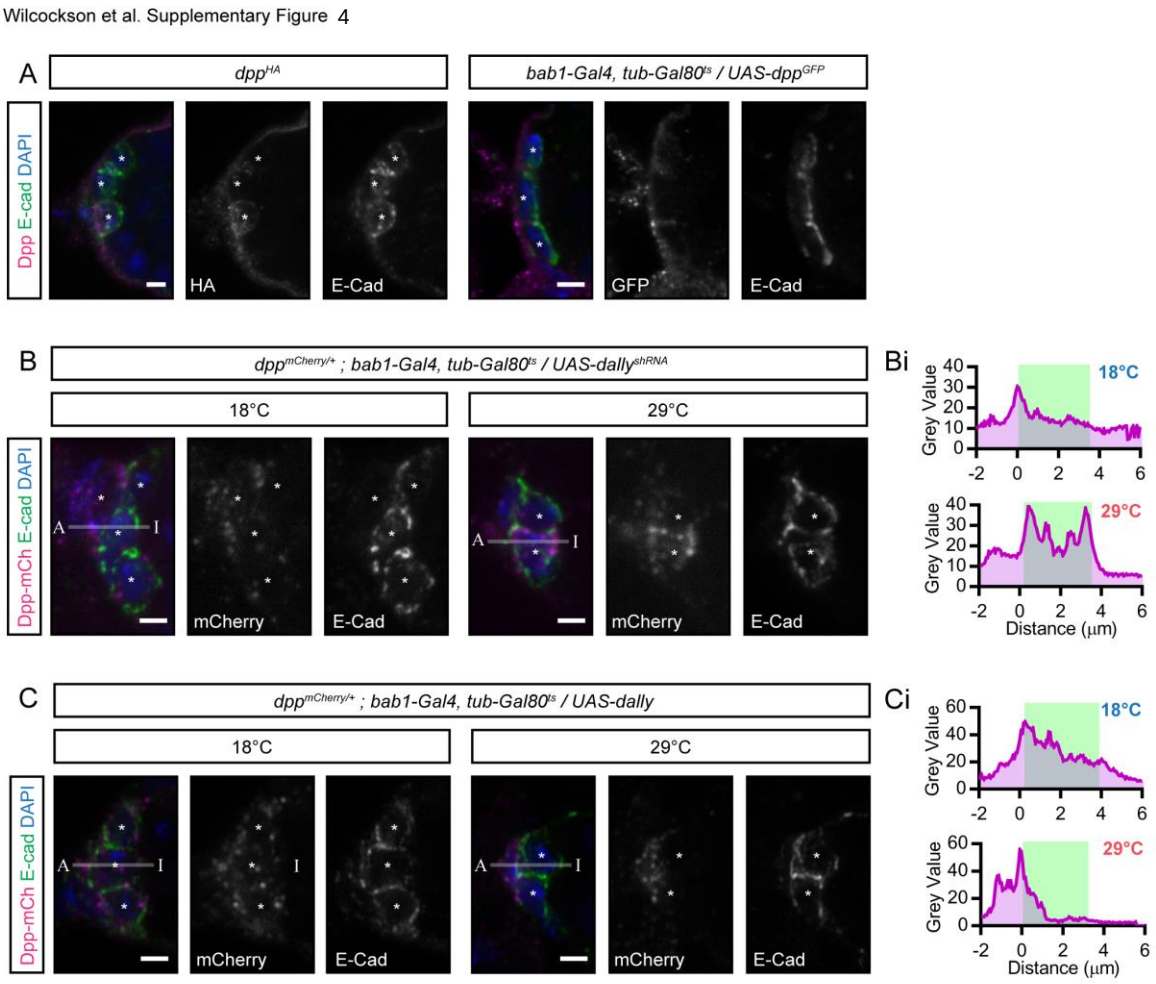

Figure S4. Niche cell-expressed Dally sequesters Dpp away from GSCs. Refers to Figure 4

(A) Extracellular immunostaining of tagged-Dpp transgenic lines; Dpp^{HA} under the control of its own promoter and UAS-Dpp^{GFP} which was transiently expressed in the anterior somatic cells of the germarium using bab1-Gal4, tub-$Gal80^{ts}$.

(B and C) Dpp^{mCh} localisation around the GSC niche following transient knockdown (B) or overexpression (C) of Dally in the anterior germarial somatic cells. Line shows where the plot of fluorescence intensity (Bi and Ci) was taken from anterior to interface (A to I) through the centre of the niche (*). E-cadherin defines the niche cell boundaries (green).

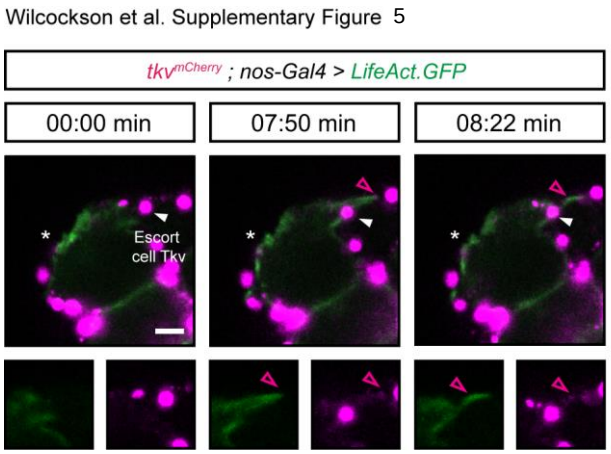

Figure S5. Lateral projections are also decorated with Tkv^{mCh}. Refers to Figure 5

(A) Stills showing F-actin labelled with *LifeAct.GFP* and endogenous mCherry-tagged Tkv showing a lateral actin-rich projection and Tkv.mCh at the tip (magenta open arrowhead). In addition, escort cell expressed 'decoy' Tkv are readily apparent in large puncta (white arrowhead) which are not connected to GSC in the first panels.

Movie S1 A dynamic cytocensor projecting into the niche. Germline expression of *UASp-eGFP.αTub*. Movie represents a maximum projection over 6µm. Time = min:sec Scale bar = 5µm. Related to Figure 2.

Movie S2 Dynamic actin-based filopodia probe the niche. Germline expression of *UASp-LifeAct.GFP*. Movie represents a maximum projection over 6.75µm. Time = min:sec. Scale bar= 5µm. Related to Figure 2.

Movie S3 All early germ cells form dynamic actin projections. Germline expression *UASp-LifeAct.GFP*. Movie represents a maximum projection over 3 µm. Time = min:sec. Scale bar= 5µm. Related to Figure 2 and S2.

Movie S4 Looking down the shaft of a filopodium extending into the niche from a lamellipodium. Germline expression of *UASp-LifeAct.GFP*. Movie represents a maximum projection over 1.5µm. Time = min:sec. Scale bar= 5µm. Related to Figure 2 and S2.